Developmental exposure to domoic acid disrupts startle response behavior and circuitry

Jennifer M. Panlilio,[1,2,3#] Ian T. Jones, [1,2] Matthew C. Salanga,[1^]
Neelakanteswar Aluru[1,3] and Mark E. Hahn[1,3]

[1]Biology Department, Woods Hole Oceanographic Institution, Woods Hole, MA 02543

[2]Massachusetts Institute of Technology (MIT) – Woods Hole Oceanographic Institution (WHOI) Joint Graduate Program in Oceanography and Oceanographic Engineering

[3]Woods Hole Center for Oceans and Human Health, Woods Hole, MA 02543

[#]Current address: Eunice Kennedy Shriver National Institute of Child Health and Human Development (NICHD), Division of Developmental Biology, Bethesda, MD 20892

[^]Current address: Department of Biological Sciences, Northern Arizona University, Flagstaff, AZ, 86011

KEYWORDS: Domoic acid; HAB toxins; developmental toxicity; startle response; escape response; startle circuit

Summary statement:

We used the zebrafish startle response as a tool to identify sensory-motor deficits and the loss of specific neural populations after developmental exposure to the harmful algal bloom toxin domoic acid.

ABSTRACT

Harmful algal blooms produce potent neurotoxins that accumulate in seafood and are hazardous to human health. Developmental exposure to the harmful algal bloom toxin, domoic acid (DomA), has behavioral consequences well into adulthood, but the cellular and molecular mechanisms are largely unknown. To assess these, we exposed zebrafish embryos to DomA during the previously identified window of susceptibility (2 days post-fertilization) and used the well-known startle response circuit as a tool to identify specific neuronal components that are targeted by exposure to DomA. Exposure to DomA reduced the probability of eliciting a startle after auditory/vibrational or electrical stimuli and led to the dramatic reduction of one type of startle, short latency c-start (SLC) responses. Furthermore, DomA-exposed larvae had altered kinematics of both SLC and long latency c-start (LLC) startle responses, exhibiting shallower bend angles and slower maximal angular velocities. Using vital dye staining, immunolabelling, and live imaging of transgenic lines, we determined that while the sensory inputs were intact, the reticulospinal neurons required for SLC responses were absent in most DomA-exposed larvae. Furthermore, axon tracing revealed that DomA-treated larvae also showed significantly reduced primary motor neuron axon collaterals. Overall, these results show that developmental exposure to DomA leads to startle deficits by targeting specific subsets of neurons. These findings provide mechanistic insights into the neurodevelopmental effects of excess glutamatergic signaling caused by exposure to DomA. It further provides a model for using the startle response circuit to identify neuronal populations targeted by toxin or toxicant exposures.

GRAPHICAL ABSTRACT

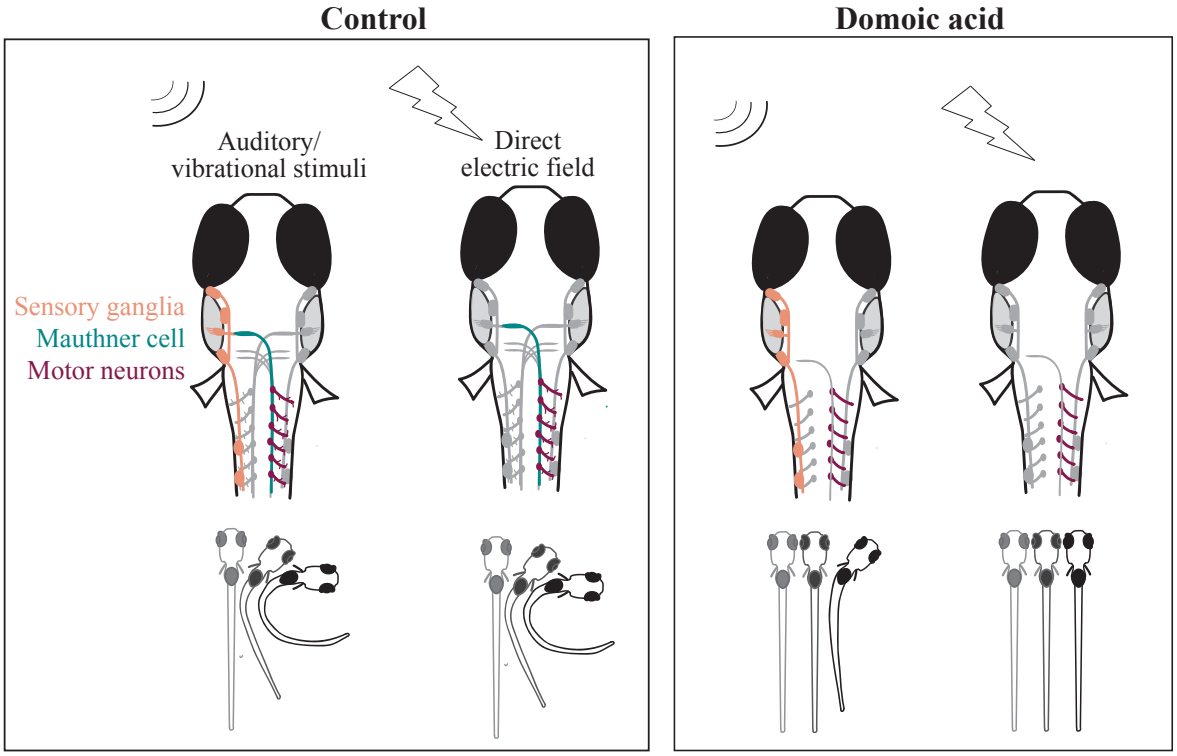

INTRODUCTION

Harmful algal blooms (HABs) – the proliferation of algae that produce toxins – have increased in frequency, duration, and geographic extent in recent decades (Anderson et al., 2002). Some HABs produce potent toxins that contaminate drinking water, seafood, and air. One such toxin, domoic acid (DomA), is produced primarily by algae in the genus *Pseudo-nitzschia.* Increasing blooms of toxic *Pseudo-nitzschia* species, resulting in part from changing climatic conditions, have been documented in recent years on both the west and east coasts of the United States, where they have led to shellfish harvest closures (Bates et al., 2018; Clark et al., 2019; McKibben et al., 2017)

DomA is a structural analog of glutamate, and is known to exert its toxicity by binding and activating ionotrophic glutamate receptors (Cendes et al., 1995; Hampson and Manalo, 1998). Exposure to DomA in adults occurs primarily through consumption of contaminated seafood. To prevent acute toxicity to humans, a regulatory limit has been set at 20 mg of DomA per kg shellfish tissue (Wekell et al., 2010). However, this limit may not be protective for earlier life stages, which are more sensitive to DomA than adult stages (Doucette et al., 2004; Tryphonas et al., 1990; Xi et al., 1997).

DomA is an established developmental neurotoxin. It has been shown to cross the placental barrier, readily accumulate in amniotic fluids, and distribute to fetal brains in non-human mammals (Brodie et al., 2006; Lefebvre et al., 2018; Maucher and Ramsdell, 2007). This provides a means by which fetuses can continue to be exposed to DomA after it is cleared from the mother's plasma (Brodie et al., 2006; Shum et al., 2020). Further exposures may occur in postnatal development through consumption of contaminated breast milk (Maucher and Ramsdell, 2005; Rust et al., 2014).

While regulatory limits to protect shellfish consumers from acute toxicity have been established, evidence shows that developmental exposures to doses of DomA that do not lead to acute neurotoxic phenotypes ("asymptomatic doses") can have long-term consequences. In rodents, both prenatal and postnatal exposures to these asymptomatic doses have been shown to lead to changes in neuron receptor densities (Perry et al., 2009), altered neural connectivity

79 (Dakshinamurti et al., 1993; Mills et al., 2016), aberrant brain morphology (Bernard et al., 2007;
80 Doucette et al., 2004; Jian Wang et al., 2000), and ultimately behavioral deficits through
81 adulthood. Behavioral deficits include impaired interlimb coordination (Jian Wang et al., 2000;
82 Shiotani et al., 2017), aberrant exploratory behavior (Levin et al., 2005; Shiotani et al., 2017;
83 Tanemura et al., 2009), reduced socialization (Mills et al., 2016; Zuloaga et al., 2016), and the
84 inability to cope with novel environments (Doucette et al., 2004; Perry et al., 2009). Many of
85 these behavioral and histological phenotypes are latent and progressive, either appearing for the
86 first time or increasing in severity as the animal ages. Developmental DomA toxicity also can be
87 silent until unmasked by further challenges such as chemical exposures in adulthood, making the
88 animals more susceptible to developing seizures and memory deficits (Gill et al., 2010; Levin et
89 al., 2005; Tiedeken and Ramsdell, 2007)
90
91 Although behavioral deficits resulting from low-level, developmental exposure to DomA have
92 been extensively characterized, the cellular and molecular mechanisms that underlie these
93 behavioral effects are poorly understood. We recently showed that exposure to DomA during a
94 specific period in zebrafish neurodevelopment (2 dpf) can lead to myelin sheath defects and
95 aberrant startle behavior, supporting the use of zebrafish as a model for investigating the cellular
96 and molecular mechanisms underlying DomA-induced developmental neurotoxicity (Panlilio et
97 al., 2020). Building on these findings by using the well-characterized startle response circuit as a
98 tool, here we i) determine which sensory and motor processes are disrupted by DomA exposure,
99 and ii) identify specific neuronal populations within the circuit that are disrupted by DomA
100 toxicity.
101
102 The startle response is an appropriate tool to investigate the behavioral effects of DomA
103 exposure. Aberrant startle response patterns have been associated with myelination defects
104 (Pogoda et al., 2006), which have been characterized as a feature of DomA toxicity (Panlilio et
105 al., 2020). In addition, aberrant glutamate signaling also alters startle response kinematics,
106 further strengthening the selection of startle response as a read-out for DomA-driven glutamate
107 excitotoxicity (McKeown et al., 2012).
108

109 Startle responses in teleosts are elicited by sudden stimuli (auditory/vibrational, tactile, visual)
110 with different intensity levels. Auditory/vibrational stimuli can lead to either of the two types of
111 startle responses– a short latency c (SLC)-type startle response or a long latency c (LLC)-type
112 startle response, which are distinguished by their onset time and kinematics. SLC responses
113 occur shortly after exposure to a stimulus (about 15 milliseconds or less, depending on
114 temperature) and tend to lead to more pronounced bend angles, while LLCs occur later and
115 produce shallower bend angles (Burgess and Granato, 2007a; Troconis et al., 2016). Increasing
116 the intensity of auditory/vibrational stimuli biases fish to perform SLC responses, which requires
117 the activation of a hindbrain neuron called the Mauthner cell (Eaton et al., 1977; Zottoli, 1977).
118 Conversely, lower intensity stimuli are more likely to lead to LLC startles, which are Mauthner
119 cell-independent (Jain et al., 2018; Marquart et al., 2019) .
120
121 The underlying startle response circuits are well known in zebrafish, making it is possible to link
122 startle behavioral data to underlying structural and cellular targets. Auditory/vibrational stimuli
123 are perceived by the statoacoustic ganglia, which transmit sensory information from the hair cells
124 in the inner ear (Faber et al., 1989; Kohashi et al., 2012). Sensory information is also perceived
125 by the lateral line, an organ system that detects vibration and changes in flow through a series of
126 mechanoreceptors along the body (Mirjany et al., 2011). For SLC startles, the statoacoustic
127 ganglia cranial nerve synapses to the Mauthner cell in the hindbrain, which fires a single action
128 potential that is propagated down its axons in the spinal cord and synapses to the primary motor
129 neurons (Kohashi and Oda, 2008; Korn and Faber, 2005). The near-simultaneous activation of
130 the primary motor neurons results in a 'c' shaped bend. In contrast to auditory/vibrational
131 stimuli, direct-electric field stimulation bypasses the sensory system altogether, directly
132 activating the Mauthner neurons and the downstream circuits (Tabor et al., 2014).
133
134 The goal of this study was to use this well-known startle response circuit as a tool to identify cell
135 targets and nervous system processes that were perturbed by DomA. We show that
136 developmental exposure to DomA reduces startle responsiveness. By varying stimulus
137 intensities, we determine whether DomA-exposed fish have the capacity to perceive changes in
138 sensory stimuli, as reflected by their increased responsiveness with higher stimulus intensities.
139 By using direct electric fields, which bypass the sensory system, we show that DomA exposed

140 fish still are unable to perform startle responses, indicating that DomA-induced startle deficits
141 occur downstream of the sensory system. Finally, with vital dyes, transgenics, and
142 immunolabeling, we identify specific neuronal populations in the startle circuit that are disrupted
143 by DomA.
144
145 **METHODS**
146 *Fish husbandry and lines used*
147 These experiments were approved by the Woods Hole Oceanographic Institution Animal Care
148 and Use Committee (Assurance D16-00381 from the NIH Office of Laboratory Animal
149 Welfare). Zebrafish (*Danio rerio*) embryos were maintained at 28-28.5°C with a 14:10 light dark
150 cycle in 0.3x Danieau's medium. The following transgenic lines were used*: Tg(mbp:EGFP-*
151 *CAAX)* (Almeida et al., 2011), *Tg(sox10:RFP)* (Kucenas et al., 2008), and *Tg(mbp:EGFP)* (gift
152 from Dr. Kelly Monk, generated by Dr. Charles Kaufman in the laboratory of Dr. Leonard Zon,
153 Harvard Medical School, Boston, MA).
154
155 *Generation of the Tg(cntn1b:EGFP-CAAX) line*
156 The *Tg(cntn1b:EGFP-CAAX)* line was generated by Gibson assembly (Czopka et al., 2013).
157 Using previously published primers, the *cntn1b* promoter region was amplified from AB
158 wildtype fish (Czopka et al., 2013). The *cntn1b* promoter was then assembled with EGFP-CAAX
159 (cloned out of *Tg(mbp:EGFP-CAAX)* fish) into the vector backbone pkHR7, which contains
160 ISCe-1 restriction sites (Hoshijima et al., 2016). To generate the stable line, the plasmid
161 containing *cntn1b:EGFP-CAAX* was co-injected along with I-SceI in the 1-2 cell stage
162 (Soroldoni et al., 2009; Thermes et al., 2002). Injected fish were grown up, and their progeny
163 that carried the transgene were used to generate embryos for experimental use.
164
165 *Domoic acid exposure paradigm (Panlilio et al., 2020)*
166 Domoic acid (5 mg; Sigma-Aldrich, MO) was dissolved directly in the vial with diluted embryo
167 medium (0.2x Danieau's) to obtain a 20 mM solution which was immediately used to generate
168 stock concentrations of 0.675 μg/μl and 1.4 μg/μl. Aliquots were then stored at -20°C. Working
169 solutions were prepared fresh prior to microinjection by diluting the stock in 0.2x Danieau's to
170 obtain the appropriate doses.

171

172 Microinjection needles were prepared from glass capillary tubes (0.58 mm inner diameter; World
173 Precision Instruments, FL; 1B100F-4) using a pipette puller (Sutter instrument model p-30, heat
174 750, pull= 0). Microinjections were then performed using Narishige IM-300 microinjector,
175 which was calibrated to consistently deliver 0.2-nL by adjusting gate time (milliseconds) and
176 back pressure.

177

178 DomA (nominal concentration of 0.14 ng) was intravenously microinjected into the common
179 posterior cardinal vein at 48-52 hpf (Panlilio et al., 2020). Controls from the same breeding
180 clutch were injected with the saline vehicle (0.2x Danieau's). To perform intravenous
181 microinjections, fish were anesthetized with 0.10% w/v Tricaine mesylate (MS222), and placed
182 laterally on dishes coated with 1.5% agarose (Cianciolo Cosentino et al., 2010). An injection was
183 deemed successful if there was a visible displacement of blood cells and no disruption of the
184 yolk during the injection process. Any fish that showed evidence of being incorrectly injected
185 were immediately removed from the study. Following injections, zebrafish were placed back in
186 clean embryo media and monitored daily.

187

188 ***Measuring Startle Responses***

189 Two different types of stimuli were used to elicit startle behavior: auditory/vibrational (A/V) and
190 direct electric field stimuli.

191

192 *Auditory/ Vibrational (A/V) stimulation*

193 A/V stimuli were generated by a minishaker (Brüel & Kjaer, Vibration Exciter 4810) connected
194 to an amplifier (Brüel & Kjaer, Power Amplifier Type 2718) (Burgess and Granato, 2007b;
195 Wolman et al., 2011). Larvae were tested in a 16-well acrylic plate (40 x 40 mm) that rested in a
196 petri dish (100mm x 100mm). The 16-well plate itself comprised of laser cut acrylic pieces that
197 were fused together using acrylic cement (Weld-On #3; IPS) (Wolman et al., 2011). An LED
198 backlight was placed below the dish to illuminate the well plate (Adafruit #1622). The petri dish
199 was epoxied to a thumbscrew (#10-32 UNF threads) that was fitted to the base of the minishaker
200 (Supplemental Fig. S1A).

201

202 Groups of larvae were subjected to four stimulus intensities (32, 38, 41, and 43 dB re 1 m/s^2) that
203 were given in increasing order (3 millisecond pulses). The software output frequency was 1000
204 Hz, though the shaker output of these pulses was more broadband, with variable peaks from 1 to
205 2000 Hz (Supplemental Fig S1B). Each stimulus intensity was given four to seven times, spaced
206 20 milliseconds apart to prevent habituation (Table S1) (Wolman et al., 2011). For a given
207 stimulus intensity, startle kinematics were shown to be statistically indistinguishable between the
208 1st and the 4th stimulus given, indicating that the 20 millisecond wait period was a sufficient
209 interstimulus interval (Supplemental Fig. S2). A high-speed video camera (Edgertronic, CA) was
210 set at a 10% pretrigger rate to capture 13 frames prior to the stimulus being elicited, while
211 recording larval movements at 1000 frames per second (Panlilio et al., 2020).
212
213 *Measuring startle vibration*
214 The startle vibration was measured as described earlier (Panlilio et al., 2020). Briefly, vibration
215 was measured using a 3-axis accelerometer (PCB Piezotronics, W356B11). The accelerometer
216 signal was low-pass filtered (10 kHz low-pass cutoff frequency) and amplified with a 30 dB gain
217 before being digitized. Data were converted into acceleration units (m/s^2) using manufacturer
218 sensitivity values for each axis of the accelerometer and accounting for gain. Data were then
219 band-pass filtered between 1 and 5000 Hz using an 8th order Butterworth filter. The Euclidian
220 norm (vector sum) for the three acceleration signals was calculated to get the total 3D magnitude
221 of acceleration. The maximum value (peak) of each impulse was calculated in decibels (dB)
222 using the following equation:
223 $$L_{z-pk} = 20 * \log_{10}(x)$$
224 where $L_{z\text{-}pk}$ is the zero-to-peak acceleration level in dB re 1 m/s^2, and x is the maximum
225 acceleration level.
226
227 *Direct electric field stimulation*
228 Larvae were head mounted in 35mm glass bottom dishes that were modified by gluing jumper
229 wires to the edges of the dish to create a defined surface area for the electric field. Larvae were
230 positioned rostral-caudally to the electrodes to provide the highest probability of eliciting a
231 startle (Tabor et al., 2014). To head-mount, fish were anesthetized in MS222 (0.16%) and
232 mounted upright (ventral side on the dish) using 1.5% low-melt agarose. Once the agarose

233 solidified, an insect pin (size #000) was used to carefully carve out the agarose so that the region
234 below the head was free to move. The dish was then flooded with embryo media (0.3x
235 Danieau's) and the fish were allowed to recover in a water bath heated to approximately 26°C.
236 Using an "embryo poker" (a piece of 0.41mm fishing line glued to a glass pipette tip), the fish's
237 tail was brushed lightly to confirm that it recovered from anesthesia prior to beginning the trial.
238 A 4.4 V/cm, 3 millisecond square wave was generated by the stimulus generator, PulsePal
239 (Sansworks, NY). This was delivered simultaneously as a TTL pulse that triggered the high-
240 speed camera (Edgertronic, CA), which recorded the tail movements at 1000 frames per second.
241 Tail bend angle and latency were then tracked using the Flote software (Burgess and Granato,
242 2007a).
243
244 *Startle behavioral analysis*
245 High speed videos were converted into jpeg files (.mov files with a minimal resolution of
246 720x720, 1/1008 shutter speed and a frame rate of 1000 frames/second). To reduce the noise and
247 tracking errors, the background was subtracted using a custom script in MATLAB (Panlilio et
248 al., 2020). Flote software (Burgess and Granato, 2007a) was then used to analyze the jpeg files.
249 Quantitative attributes of the startle response measured include startle responsiveness (whether
250 larvae responded or not), latency (time between stimulus and startle), bend angle and maximal
251 angular velocity during startle (Panlilio et al., 2020).
252
253 *Using mixture models to identify latency cut-offs for SLC versus LLC responses*
254 In response to auditory/vibrational stimuli, zebrafish perform two types of startle responses:
255 short latency c-bends (SLCs) and long latency c-bends (LLCs) (Supplemental Fig S1C). These
256 two types of startle responses have different latencies, distinct kinematics, and are driven by
257 separate underlying neural circuits (Burgess and Granato, 2007a; Burgess and Granato, 2007b;
258 Higashijima et al., 2003; Marquart et al., 2019). To distinguish between the two types of startle
259 responses, we identified a latency cutoff using a Gaussian mixture model, which fitted two
260 Gaussian distributions, and assigned each latency data point a probability of belonging to either
261 of the two distributions (R package, mixtools) (Benaglia et al., 2009; Panlilio et al., 2020). The
262 cut-off for assigning a response as an SLC was 14 milliseconds – the latency with a greater than

263 50% probability of belonging to the first fitted Gaussian distribution (Supplemental Fig. S1D).
264 Startle responses that had latencies greater than 14 milliseconds were classified as LLCs.
265
266 *Statistical modeling of startle responsiveness*
267 Every fish was given 4-7 replicate auditory/vibrational stimuli per each stimulus intensity tested.
268 For all instances where a fish was successfully tracked, response rates were recorded. Response
269 rates for individual fish were calculated (% responsiveness = number of times the fish responded
270 / number of successfully tracked videos with a maximum of 4 tracks per stimulus intensity per
271 individual fish). A mixed effects logistic regression model was then used to identify treatment
272 differences in percent responsiveness, with the treatment as a fixed effect and the replicate
273 experimental trials as a random effect (glmer(), lme4 R package) (Bates et al., 2015).
274
275 *Imaging myelin sheaths in the spinal cord following domoic acid exposures*
276 Our previous results (Panlilio et al., 2020) showed pronounced myelin defects following
277 exposures to DomA at 2 dpf. To determine whether there is a relationship between the behavioral
278 findings and the myelin phenotype, *Tg(mbp:EGFP-CAAX)* embryos were exposed to DomA at 2
279 dpf and screened for myelin defects prior to behavioral analyses at 7 dpf. The severity of the
280 myelin defect was qualitatively scored (Supplemental Fig. S3). To simplify the analyses, four
281 categories were used (Panlilio et al., 2020): (0) Normal phenotype — dorsal and ventral regions
282 had labeled myelin sheaths. The myelin sheath surrounding the Mauthner axon was visible. (1)
283 Myelin sheaths were present but disorganized. In some cases, myelinated axons that were
284 normally found ventrally were located more dorsally. In others, the myelinated axons terminated
285 prematurely with distal ends located more dorsally. (2) Myelin was labeled in both the dorsal and
286 ventral regions of the spinal cord, but there are some noticeable deficits. While the ventral spinal
287 cord was labeled, it had noticeably less myelin labeled compared to controls. (3) The loss of
288 labeled myelin in the ventral spinal cord resulted in large, observable gaps between myelinated
289 axons. Circular myelin membranes were present both in the ventral and dorsal spinal cord.
290
291 *Statistical modelling of the distribution of startle response type due to treatment*
292 When fish responded to a stimulus, they either performed an SLC or an LLC startle which was
293 defined by the latency cut-off of 14 milliseconds. To determine whether domoic acid exposure

294 alters the proportion of SLC to LLC responses, a mixed effects logistic regression model was
295 used with treatment as a fixed effect and the replicate experimental trials as a random effect.
296
297 DomA-exposed fish were also classified by the severity of myelin defects. To determine whether
298 there is an association between the myelin severity and the likelihood that a fish performs an
299 SLC rather than an LLC, a separate mixed effects logistic regression model was used, with
300 myelin severity as the fixed effect and the replicate experimental trials as a random effect.
301
302 *Calculating the Startle Bias Index*
303 The Startle Bias Index was calculated as described previously (Jain et al., 2018). Bias per
304 individual fish was calculated as the (frequency of SLC – frequency of LLC)/ total responses
305 where +1 represents the value in which all responses were SLC startles, and -1 represents the
306 value in which all were LLC startles. Following this, mean behavioral biases for a treatment
307 group were calculated.
308
309 *Analysis of treatment differences in startle response kinematics (Panlilio et al., 2020)*
310 Kinematic responses from the two types of startle responses (SLC v. LLC) were analyzed
311 separately based on previous research showing that they are driven by distinct neural circuits and
312 have distinct kinematic characteristics (Burgess and Granato, 2007b; Marsden and Granato,
313 2015; O'Malley et al., 1996). The median response of individual fish for each startle type was
314 then calculated for each intensity level.
315
316 To determine whether DomA alters kinematic responses to startle, we performed Aligned
317 Ranked Transformed ANOVA test, with treatment group as a fixed factor (DomA vs. control).
318 Nine separate repeated experiments (trials) were combined for the analysis (art(), ARTool R
319 package) (Wobbrock et al., 2011) (Table S1). To account for potential differences in response
320 due to the variations between trials, the experimental trial was incorporated into the model as a
321 random factor.
322

323 To determine whether there was an association between the myelin phenotypes and the startle
324 kinematics, we used a nonparametric multiple comparisons test with Dunnett-type intervals
325 (nparcomp(), nparcomp R package) (Konietschke et al., 2015).
326
327 *Immunohistochemistry*
328 Fish were fixed in 4% paraformaldehyde overnight at 4°C. In some cases, whole brains were
329 dissected, and in other cases whole embryos were used. Antigen retrieval was done by placing
330 tissue in 150 mM Tris HCl (pH 9.0) in a 70°C water bath for 15 minutes (Inoue and Wittbrodt,
331 2011). Brain tissue was permeabilized using proteinase K (10 μg/ml for 3 minutes) then post-
332 fixed for 20 minutes using 4% paraformaldehyde. Whole mount embryos were permeabilized
333 using ice-cold acetone (7 minutes). Samples were then blocked in 10% normal goat serum and
334 1% DMSO, followed by 1-3 day incubations in primary antibodies (α-3A10 -1:100 dilution,
335 Developmental Studies Hybridoma Bank, antibody registry ID: AB 531874, prepared 7/28/16,
336 51 μg/ml; α-acetylated tubulin – 1:500 dilution, Santa Cruz Biotechnology, SC 23950 sample
337 HS417, 10 μg/ 50 ml). After several washes in phosphate buffered saline with 0.01% triton-X,
338 samples were then incubated in secondary antibodies (1:400 Alexa Fluor 488 Goat α-mouse,
339 Catalog A11001, 1752514 or Alexa Fluor 594 Goat α-mouse; Abcam, GR196875). Samples
340 were then placed in antifade mountant (Prolong or SlowFade Diamond mountant, Invitrogen),
341 and placed between bridged #1.5 coverslips for imaging.
342
343 Acetylated tubulin was used to assess primary neuron axons, early sensory neurons (Rohon beard
344 cells), and the peripheral lateral line, while 3A10 was used to characterize Mauthner cell bodies
345 and hindbrain and midbrain axonal tracks. Brain dissections required for 3A10 staining
346 sometimes led to reticulospinal axons (those that extend down to the spinal cord) being removed
347 from the preparation. (Supplemental Fig. S4 shows the range of phenotypes found in controls).
348 Thus, for the antibody labeling experiment, the presence or absence of the Mauthner cell was
349 determined solely based on the presence of the Mauthner cell body and lateral dendrite.
350
351 *DASPEI labeling*
352 Sensory neuromasts were labeled using the vital dye, DASPEI ((2-(4-(dimethylamino)styryl) -N-
353 ethylpyridinium iodide, Biotium Inc., Freemont, CA). Zebrafish larvae (5 dpf) were incubated in

354 0.005% DASPEI for 15-20 minutes, then washed and placed in anesthetic (0.16% MS222).
355 Larvae were then mounted in low-melt agarose (1-1.5%) either laterally or ventrally and imaged
356 with a widefield microscope. Neuromasts were manually counted on blinded files. To identify
357 treatment differences in counts, a random coefficient Poisson regression was done, with repeated
358 experiments (trials) modeled as a random factor (glmer(), lme4 R package) (Bates et al., 2015).
359
360 *Reticulospinal backfills*
361 Larvae (7 dpf) were anesthetized using MS222 (0.16%), then mounted ventrally in 1.5% low
362 melt agarose. Dissection spring scissors were dipped into Texas red dextran (3000 MW) and the
363 spinal cord was transected at the level of the anus (Moens et al., 1996). Larvae were placed back
364 into anesthetic and screened for dye uptake using epifluorescence microscopy (Zeiss Axiovert
365 inverted microscope). Roughly an hour after spinal cord transections, larvae were placed in 4%
366 paraformaldehyde and fixed overnight in 4°C. Following several washes in PBS, the whole brain
367 was dissected (Turner et al., 2014). Whole brains were mounted using the same technique used
368 with brains that were labeled with antibodies. The presence of the Mauthner cell, along with any
369 labeled neurons in rhombomere 5 (r5) and rhombomere 6 (r6) – the location of MiDcm2,
370 MiDcm3 – was identified. Following this classification, ordered logistic regression was done to
371 determine whether treatment alters the number of neurons found in each location (polr(), Mass R
372 package, R) (Ripley et al., 2018).
373
374 *Primary motor neuron live imaging and tracing*
375 *Tg(cntn1b:EGFP-CAAX)* embryos were exposed to DomA at 48-53 hpf. Larvae (2.5 dpf) were
376 then anesthetized (0.16% MS222), and embedded laterally in 1-1.5% low-melt agarose in glass
377 bottom microscopy dishes. Larvae were imaged using a confocal microscope (LSM 710 or LSM
378 780) with the 40x water immersion objective (C-Apochromat, 40x, NA 1.1). Primary motor
379 neurons located approximately at myotome 20-23 were imaged. Images were blinded prior to
380 image analysis. A single primary motor neuron from the image stack was chosen. Its main axon
381 along with the axon collaterals were traced from the image stacks using the ImageJ plugin,
382 Simple Neurite Tracer (Longair et al., 2011). The total length of the traced axon collaterals was
383 calculated from the tracing files. One-way analysis of variance was used to determine whether
384 there was an effect of treatment on the total length of the axon collaterals (oneway.test(), R).

385
386 **RESULTS**

387 *DomA-exposed fish were less responsive, and less likely to perform SLC startles*

388 We first determined whether DomA alters responsiveness over the range of stimulus intensities
389 tested. At the lowest stimulus intensity (32 dB), most control and DomA-treated fish did not
390 respond (Fig. 1A, Table S2). Furthermore, both DomA and control fish that did respond were
391 more likely to perform LLCs rather than SLC startles. While this was true for both control and
392 DomA-exposed fish, DomA-exposed fish were even less likely to respond (Estimate = -0.474,
393 p=0.0132, Table S3), and even less likely to perform SLC startles rather than LLC startles
394 compared to controls (Estimate = -1.076, p=5.84E-15, Table S4).
395
396 With higher stimulus intensities (≥38 dB), a greater proportion of both the control and DomA-
397 treated fish performed startles rather than not responding (Fig. 1A, Table S2). However, as seen
398 at the lowest stimulus intensity, DomA-exposed fish were significantly less likely to respond and
399 significantly less likely to perform an SLC startle vs. a LLC startle, compared to control fish
400 (Tables S3 and S4).
401
402 SLC loss is further illustrated by calculating the *startle bias index* (Jain et al., 2018), a measure
403 of the frequency with which individual fish performed an LLC versus an SLC response at a
404 given stimulus intensity. At intensities of 38 dB and higher, control fish preferentially performed
405 SLC rather than LLC responses (Fig. 1B). In contrast, DomA-exposed fish preferentially
406 performed LLC rather than SLC responses at all stimulus intensities tested.
407

408 *Fish with myelin defects were less likely to perform SLC startles than those without defects*

409 Previously, we showed the DomA-exposed larvae had myelin deficits (Panlilio et al., 2020). To
410 assess the relationship between startle bias and the observed myelin sheath defects, we classified
411 a subset of the larvae based on myelin defects prior to the behavioral assessment. Similar to the
412 controls, DomA-exposed fish with normal myelin sheaths (category 0) performed more SLC
413 startles at higher stimulus intensities (38 dB and higher) and did not differ from controls in the
414 likelihood of performing LLCs over SLCs at the highest intensity tested (43 dB) (Fig. 1C, Table
415 S5). In contrast, fish with any noticeable myelin defects (Category 1-3) had a reduced likelihood

416 of switching from LLC to SLC startles with increasing stimulus intensity, as compared to
417 controls ($p < 0.0004$, Table S5). Furthermore, DomA-exposed fish with the most severe defects
418 (Category 3) were also less likely to switch from LLC to SLC startles at 43 dB compared with
419 DomA-exposed fish with any of the less severe myelin defects (Category 0-2) (Estimate= -3.196
420 for DomA-exposed fish (Category 3) = -3.1957, p= 4.81E-14; Table S5).
421
422 *DomA-exposed fish that had myelin defects also had startle response kinematic deficits*
423 For the fish that responded to a given stimulus, the startle kinematics (bend angle, maximal
424 angular velocity) were assessed. In agreement with our previous findings (Panlilio et al., 2020),
425 DomA-exposed animals had smaller bend angles and lower maximal angular velocities (Mav)
426 compared to control animals at all the intensities tested (Supplemental Fig. 5; $p < 2.22$ e-16).
427 This was true for both LLC (Supplemental Fig. 5A, B; Table S6) and SLC (Supplemental Fig.
428 5C, D) startles.
429
430 We then determined whether myelin defect severity was correlated with startle kinematic
431 performance. A majority of DomA-exposed larvae were classified as category 3 (the most severe
432 myelin defects). When performing either SLC or LLC startle responses, these larvae had
433 significantly reduced bend angles and Mavs for all stimulus intensities tested (Fig. 2).
434
435 Fish with intermediate myelin defects (category 1-2) also consistently had kinematic deficits
436 when performing SLC startles across all stimulus intensities tested (Fig. 2A, 2B, Table S6).
437 However, it was only fish with the most severe myelin defects (category 3) that had reduced
438 bend angles and slower maximal angular velocities during LLC startles (Fig. 2C, 2D, Table S7).
439
440 Like DomA-treated fish in other categories, DomA-treated fish with control-like myelin sheaths
441 (category 0) also had kinematic deficits when performing SLC startle responses (Fig. 2A, 2B,
442 Table S6). In contrast, DomA-treated fish with category 0 phenotypes did not have any
443 measurable kinematic deficits when performing LLC startle responses at all stimulus intensities
444 tested (Fig. 2C, 2D, Table S7).
445

446 These results suggest that exposures to DomA that led to distinguishable myelin defects also led
447 to startle deficits. The severity of the myelin defect was correlated with the severity of the
448 behavioral deficit; fish with the most severe myelin defects were also less likely to perform SLCs
449 and had shallower bend angles and slower maximal angular velocities relative to controls.
450
451 *DomA-exposed fish were less responsive, and had aberrant kinematics following direct-electric*
452 *field stimulation*
453 To assess the contribution of the sensory system to the observed startle deficits, we used direct
454 electric field stimulation, which bypasses the sensory system, directly activating the Mauthner
455 cell, leading to ultra-rapid startle responses (Tabor et al., 2014) (Fig. 3A). DomA-treated larvae
456 were significantly less responsive to electrical stimulation than control fish ($p < 1$ e-16). A
457 majority of control fish (70/74) responded to all of the 7 replicate stimuli (Fig. 3B), while a
458 majority of the DomA-treated fish (47/74) did not respond to any of the replicate stimuli.
459 Furthermore, control fish responded rapidly to electrical stimulation, with a median latency of 2
460 milliseconds (Fig. 3C). Strikingly, when DomA-treated fish did respond, they had significantly
461 longer latencies (control median = 2 ms, DomA median= 49 ms, IQR= 2 s, estimated relative
462 effect (est) = 0.78, 95% CI [0.633, 0.927], p=0.001). When DomA-treated fish did respond, they
463 also had shallower bend angles and slower maximal angular velocities compared to controls
464 (bend angle: median =83.5° in controls, median = 41.9° in DomA-treated, Coefficient= 0.173,
465 95% CI [0.059, 0.286], $p <$ e -16; mav: median = 3.78 °/ms in controls, median = 2.28 °/ms in
466 DomA treated, Coefficient = 0.21, 95% CI [0.083, 0.338], $p <$ e -16) (Fig. 3D and 3E).
467
468 Like auditory/vibrational startle deficits, deficits in electric field-induced startle were also
469 correlated with myelin defects; DomA treated fish with more severe myelin defects also had
470 more deficits in startle (Fig. 4). DomA-treated fish that had no visible myelin defects had no
471 differences in responsiveness, bend angles, Mavs, or latencies compared to controls (Fig. 4A-E).
472 In contrast, DomA-treated fish with any visible myelin defect, even in its least severe form
473 (category 1), had significantly reduced responsiveness compared to controls (Dunnet post-hoc
474 test, $p <$ e -9) (Fig. 4E). Furthermore, DomA-exposed fish that had defects of intermediate
475 severity (category 2) also had significantly longer latencies (est= 0.989, 95% CI= [0.946, 1.032],
476 p<3.28 e -13), but no statistically significant differences in bend angle or Mav (Fig 4C, 4D;

477 Table S8). Finally, DomA-exposed fish that had the most severe myelin defects (category 3) had
478 deficits for all startle attributes measured (Fig. 4A-E; Table S8).
479
480 To further identify the potential cellular and structural defects underlying these observed
481 behavioral deficits, we imaged different components of the startle circuit, starting with the
482 sensory system.
483
484 *Sensory inputs for acoustic/vibrational startle*
485 We assessed the key sensory inputs that are required for performing auditory/vibrational startle
486 responses. When an auditory/vibrational stimulus is provided, hair cells in the inner ear, and in
487 some circumstances within neuromasts in the lateral line, are activated. When activated, these
488 hair cells lead to the activation of the statoacoustic ganglia (in the inner ear) or the lateral line
489 ganglia, which in turn send the sensory information to the hindbrain where the information is
490 integrated (Nicolson, 2017; Nicolson et al., 1998). To assess whether DomA disrupts the sensory
491 system, we sought to determine whether DomA reduced the number of neuromasts or disrupted
492 statoacoustic ganglia or lateral line structures.
493
494 Using the vital dye DASPEI, we labelled the neuromasts and found no differences in the number
495 of neuromasts in both the cranial and the trunk region after exposure to DomA (Fig. 5A,B). By
496 exposing transgenic *Tg(cntn1b:EGFP-CAAX)* fish, in which the peripheral lateral line and the
497 statoacoustic ganglia are labeled, we also found no discernible differences in the presence of
498 these structures compared to controls (Fig. 5D,E).
499
500 *Reticulospinal neurons integrate sensory information*
501 To determine whether DomA disrupts hindbrain neurons responsible for integrating sensory
502 information, we performed spinal backfills. This allowed us to label the Mauthner cells – paired
503 neurons required for eliciting SLC responses – and their homologs MiDcm2 and MiDcm3, which
504 are active during LLC responses (Marsden and Granato, 2015; O'Malley et al., 1996). Most of
505 the control larvae had both Mauthner cells and all four neurons within rhombomere 5 (r5) and
506 rhombomere 6 (r6), the position where MiDcm2 and MiDcm3 reside (Fig. 6). In contrast, a
507 majority of DomA-exposed larvae had neither Mauthner cell, and 0 or 1 (out of the 4) neurons in

508 positions r5 and r6 (Fig. 6A-C). In fact, fish exposed to DomA were 99.3% less likely than
509 controls to have both Mauthner cells rather than 1 or 2 Mauthner cells (odds ratio (OR) = 0.007,
510 p = 1.7 e -14), and had an even lower probability of having 4 neurons in r5 and r6 (OR = 0.001,
511 p= 1.6 e -09).
512
513 Spinal backfills have some disadvantages. While the absence of labeled neurons may be an
514 indication that the neurons are not present, it is possible that the neurons are present but may not
515 have axons that extend to the cut site where the axons can take up dye. Furthermore, if neurons
516 have defective axonal transport mechanisms, their axons may be present but unable to take up
517 the dye efficiently enough to stain their cell bodies. To address these potential pitfalls, we also
518 performed whole brain 3A10 antibody staining, which labels the Mauthner cell bodies along with
519 other midbrain and hindbrain axonal tracks (1-7) (Fig. 7A). In agreement with the spinal backfill
520 data, a majority of DomA-exposed larvae did not have Mauthner cell bodies, while a majority of
521 controls did (Fig. 7B and 7C). Importantly, other axonal tracts in the midbrain and hindbrain
522 appeared to be intact in both control and exposed animals. Both control and DomA-exposed
523 animals had medial longitudinal fasciculi, and there were no significant differences in the
524 number of hindbrain axonal tracts (Fig. 7B and 7D).
525
526 *Primary motor neurons that innervate muscles that generate the response*
527 We then determined whether DomA disrupts primary motor neurons that synapse with the
528 hindbrain reticulospinal neurons and innervate the muscles required to elicit startle. To determine
529 whether DomA alters the main primary motor neuron axons, we stained the trunk region using α-
530 acetylated tubulin (Fig. 8A). There were no differences in the presence of the primary motor
531 neurons in DomA-exposed larvae versus controls (Fig. 8B,C). In the same tissue, there were also
532 no differences in the appearance of sensory neuron cell bodies or the peripheral lateral line (Fig.
533 8B,C).
534
535 By using the transgenic line *Tg(cntn1b:EGFP-CAAX),* we were then able to examine the axon
536 collaterals that branch from the main caudal primary motor neuron axon. While staining with α-
537 acetylated tubulin showed no differences in the presence of the main branches in primary motor
538 neurons (Fig. 8D), tracings of the motor neuron axon collaterals in DomA-treated

539 *Tg(cntn1b:EGFP-CAAX)* larvae showed a significant reduction in the length of the branches
540 (Fig. 8E, 8F) (Control (mean ± SE) = 1457 μm ± 43, DomA (mean ± SE) = 527 μm ± 29, $F(1, 74.6) = 315.87$, $p < 2.2\ e\text{-}16$).
541
542
543 **DISCUSSION**
544 Developmental exposure to DomA leads to persistent behavioral deficits, but the cellular and
545 molecular mechanisms that underlie these effects are largely unknown. We used the zebrafish
546 model and its well-characterized startle response circuit as tools to identify the cell types that are
547 preferentially targeted by developmental DomA exposure and link these to sensorimotor
548 processing deficits that occur during startle. Our results reveal that DomA exposure alters
549 sensorimotor function, reducing responsiveness to stimuli and disrupting kinematics during
550 startle. By imaging the neuronal components of the circuit, we found that DomA exposure led to
551 the loss of reticulospinal neurons and to the reduction in axon collaterals in caudal primary motor
552 neurons, while not affecting the presence of sensory ganglia or other hindbrain axon tracks.
553 Taken together, these results suggest that DomA exposure leads to the loss of specific cells that
554 are necessary for startle circuit function, resulting in behavioral startle deficits.
555
556 *Mauthner cells are targeted by DomA exposure*
557 DomA prevents specific types of startle response from occurring in a manner consistent with the
558 loss of a type of hindbrain reticulospinal neuron known as the Mauthner cell. The Mauthner cell
559 is required for performing both electric field-induced startle and A/V-induced SLC startles (but
560 not LLC startles) (Kohashi and Oda, 2008; Marsden and Granato, 2015; Tabor et al., 2014).
561 Behaviors that require the Mauthner cell-mediated startle were lost in a majority of the DomA-
562 exposed larvae. Furthermore, DomA exposed larvae preferentially performed LLC startles versus
563 SLC startles even with high intensity A/V stimuli. These behavioral results suggest that the
564 Mauthner cell is disrupted by DomA. Imaging results supported this; using two complementary
565 approaches (spinal backfills and antibody staining for the neurofilament 3A10) we confirmed
566 that the Mauthner cells were absent in a majority of DomA-treated larvae.
567
568 *DomA-induces motor axon collateral loss*

569 DomA-exposed larvae showed kinematic deficits such as smaller bend angles and slower Mavs
570 when performing all forms of startle tested (SLC, LLC, and electric field-induced startles). We
571 hypothesized that this shared phenotype (altered startle kinematics) may be a result of
572 disruptions to a cell type that is common in the neural circuits of these three types of startle
573 responses. One of the shared neuronal components is the downstream primary motor neuron that
574 activates the trunk and tail muscles required for the startle responses. While the main caudal
575 primary motor neuron axons were present in DomA-exposed fish, the collaterals of these motor
576 neuron axons were severely reduced. The reduction in the collaterals translated to fewer synapses
577 to the trunk muscles, would could consequently have led to the observed shallower bend angles
578 (McLean and Dougherty, 2015).
579
580 *Sensory system is an unlikely primary target for DomA*
581 Developmental DomA exposure does not completely disrupt sensory processing during startle,
582 consistent with the morphological data showing intact sensory ganglia. The sensory system is
583 bypassed following direct-electric field stimulation, and yet DomA-exposed larvae still exhibited
584 kinematic deficits under these conditions. This result indicates that the observed behavioral
585 deficits cannot be due to solely deficits in the sensory system. Furthermore, while DomA-
586 exposed larvae responded less often than control larvae, they still had the capacity to respond to
587 A/V stimuli. Their responsiveness increased with increasing stimulus intensities, suggesting that
588 DomA-exposed larvae have the ability to encode graded sensory information that translates to
589 different degrees of responsiveness. Indeed, when assessing different components of sensory
590 circuit, we found that DomA did not reduce the number of neuromasts or disrupt the presence of
591 important sensory ganglia necessary for perceiving A/V stimuli, supporting the idea that DomA
592 may not disrupt sensory system structures.
593
594 Importantly, we only assessed the presence versus absence of the specific sensory structures
595 rather than their function. Previous studies have shown that the application of the ionotropic
596 glutamate receptor agonist, AMPA, reduced the firing of afferent sensory neurons and the
597 neurons' responsiveness to hair cell activation (Sebe et al., 2017). Furthermore, we only assessed
598 gross morphological features: we quantified the number of neuromasts present rather than more
599 detailed structural features such as number of hair cells within a neuromast or the number of

600 branches in afferent neuron terminals that synapse to the hair cells. Indeed, zebrafish hair cells
601 express AMPA and KA receptors to which DomA binds (Hoppmann et al., 2008), making them
602 potential targets for toxicity. Exposure to high doses of ionotropic glutamate agonists have been
603 shown to lead to both the loss of hair cells within a single neuromast (with 300 μM KA or
604 AMPA) (Sheets, 2017), and to the swelling of hair cell afferent synapses (with 100 μM AMPA)
605 (Sebe et al., 2017).
606
607 It is conceivable that DomA may bind to ionotropic glutamate receptors in hair cells and at the
608 mature hair cell ribbon synapse. DomA-induced overactivation of these receptors could then lead
609 to hair cell death with individual neurons, and to the reduced firing capacity of afferent sensory
610 neurons. Both of these events could contribute to the reduced responsiveness observed in DomA-
611 exposed larvae. However, a more detailed analysis of individual hair cells and hair cell afferent
612 synapse following DomA exposure would be necessary to determine whether this occurs.
613
614 Taken together, these results indicate that DomA does not alter the overall structures in the
615 sensory system, nor does it affect the ability of larvae to increase their responsiveness with
616 higher stimulus intensities. However, DomA-exposed fish are generally less responsive relative
617 to control fish, which may be due to subtle perturbations to sensory systems that have yet to be
618 investigated.
619
620 *Behavioral deficits are correlated with the severity of myelin phenotypes*
621 The startle circuit is heavily myelinated to achieve rapid signaling. We showed previously that
622 myelination deficits result from developmental exposure to DomA (Panlilio et al., 2020). By
623 imaging *Tg(mbp:EGFP-CAAX)* larvae prior to behavioral tests, we were able to correlate the
624 degree of myelin severity to the behavioral phenotypes.
625
626 We found that fish with more severe axonal and myelin defects were also likely to have more
627 severe startle deficits. EGFP expression in *Tg(mbp:EGFP-CAAX)* fish was a proxy for the
628 degree (score) of axonal and myelin defects because its expression is dependent both on intact
629 myelin and on the presence of the axons (with no axons, there is nothing for oligodendrocytes to
630 myelinate). Imaging results (Fig. 6 and 7) indicated that by the larval stages, reticulospinal

631 neurons are lost in DomA-exposed fish, suggesting that the aberrant EGFP expression at these
632 later developmental stages is due to the loss of axons. However, we cannot exclude the
633 possibility that the loss of these axons was secondary to, or exacerbated by, the myelination
634 defects. Our previous work (Panlilio et al., 2020) showed that as early as 2.5 dpf – the time at
635 which axons are first wrapped – myelination is already perturbed. Thus, future studies are
636 necessary to see whether DomA targets the axons first, followed by the myelination, or whether
637 the loss of myelin leads to the axonal defects later.
638
639 Using EGFP labeling of myelin as a proxy for axonal and myelin integrity, we were able to
640 determine that behavioral deficits observed were largely correlated to the severity in axon and
641 myelin defects. Indeed, DomA-exposed larvae with "control-like" axons and myelin sheaths had
642 fewer kinematic deficits relative to DomA-exposed fish with axon or myelin defects. However,
643 there were some behavioral attributes for which this was not true. Fish with "control-like" axons
644 and myelin did not always have "control-like" kinematics, especially during SLC startles. There
645 are two potential explanations for this. 1) Fish that had "control-like" myelin sheaths and axons
646 may have subtle myelin sheath and axonal defects that we could not distinguish from controls at
647 the resolution we were imaging. These subtle defects could contribute to some of the observed
648 SLC kinematic deficits. 2) Alternatively, DomA-exposed fish had myelin sheaths and axons that
649 were indistinguishable from controls, but may have had other neuronal defects that we did not
650 assess in relation to the behavioral changes. To test the latter scenario, future work could be done
651 to assess the subset of the fish that had "control-like" myelin sheaths for effects on other cell
652 targets, including motor axon collateral branching and ionotropic glutamate receptor activity in
653 hair cells.
654
655 *DomA is not just a general neurotoxin*
656 More generally, these findings suggest that DomA isn't simply a nonspecific neurotoxin that
657 targets all neural precursors and neurons, but instead one that targets specific neuronal and glial
658 subtypes. The most apparent targets of DomA were the reticulospinal neurons in the hindbrain
659 (including the Mauthner cell) and the caudal primary motor neurons. DomA had no apparent
660 effects on other neurons and neuronal precursors examined including the medial longitudinal
661 fasciculus, the hindbrain axonal tracts, the Rohon-beard sensory cell bodies, or the neural

662 precursors in the spinal cord. While both Mauthner cells and caudal primary motor neurons
663 express the ionotrophic glutamate receptors to which DomA binds (Patten and Ali, 2007; Todd et
664 al., 2004; Warp et al., 2012), so too do other neurons and glial cells (Hoppmann et al., 2008),
665 suggesting that other factors may be important in mediating susceptibility of subclasses of
666 neurons.
667
668 The sensitivity of hindbrain reticulospinal neurons and motor neurons to DomA may be due to
669 their intrinsic properties. Both of these neuron types have large axons, some with extensive
670 axonal arbors that are located in either the spinal cord or periphery (Kimmel et al., 1982; Myers,
671 1985). Any perturbation that disrupts homeostatic mechanisms, such as slowing of axonal
672 transport, could have important effects on these neurons, making these cells more susceptible to
673 disease and environmental insults. In fact, motor neurons are known for being selectively
674 vulnerable to insult because they are large, continuously active and heavily rely on mitochondrial
675 respiration processes (Lewinski and Keller, 2005).
676
677 *Implications for human health*
678 Finally, while these studies were done in zebrafish, these findings have implications for human
679 health. Behavioral data indicate that DomA exposure in fish disrupts motor control. Motor
680 deficits have been previously characterized from both incidental human exposures and animal
681 exposure models (Shiotani et al., 2017; Teitelbaum et al., 1990; Wang et al., 2000). Adult
682 humans acutely exposed to DomA developed sensorimotor neuropathy and axonopathy as
683 assessed by electromyography (Teitelbaum et al., 1990). A subset of primates exposed orally at
684 or near the accepted daily tolerable dose of 0.075 mg/kg developed visible hand tremors (Petroff
685 et al., 2019). Rodents prenatally exposed to DomA (PND 10-17) developed aberrant gait patterns
686 (Shiotani et al., 2017). These results suggest that motor deficits may be an important functional
687 endpoint for DomA toxicity; future studies should assess both reflex and fine motor skills. One
688 recent study in non-human primates found that *in utero* exposure to DomA had no impact on
689 early survival reflexes in neonates (Grant et al., 2019). It would be useful to continue to trace
690 motor skill development in these neonates to determine whether there are any potential latent
691 effects, or whether more subtle motor skill deficits emerge.
692

693 The study also provides insights into potential cell targets for developmental exposures to
694 DomA, demonstrating that DomA selectively targets specific neurons – the primary motor
695 neurons and reticulospinal neuron subclasses. While humans do not have Mauthner cells, the
696 intrinsic characteristics that make this cell type more vulnerable to toxins may be shared with
697 other neurons in humans. Identifying these general characteristics (large axons, extensive arbors,
698 location in the spinal cord) may also provide some useful hints as to which neurons are targeted
699 in humans. While the identification of other candidates would require other animal models, our
700 results using the zebrafish startle response can help guide further investigation of the cellular and
701 molecular mechanisms underlying the behavioral deficits caused by early life exposure to
702 DomA.
703
704 **CONCLUSION**
705 This study characterized the effects of developmental DomA exposure on the startle response.
706 The startle response circuit is well characterized, and the neural circuits that drive it are well
707 known. Utilizing this knowledge, we were able to identify specific neural populations that may
708 be more sensitive to early life exposure to DomA. Furthermore, this study illustrates the potential
709 of using the startle response circuit as a tool to identify neuronal populations targeted by toxin or
710 toxicant exposures.
711
712 **ACKNOWLEDGEMENTS**
713 We thank H.E. Rivera and A.R. Solow for their advice on the statistical analysis, H.A. Burgess
714 for providing the Flote software for startle kinematic analysis, B.G. Merrick for his help
715 designing and building the startle apparatus, and N.R. Brun and L. Kerr for microscopy training
716 and advice (MBL microscopy facility). We also thank the labs who generously provided us with
717 zebrafish transgenic lines to make this work possible: B. Appel (University of Colorado,
718 Denver), K.R. Monk (Oregon Health & Science University), C.K. Kaufman (Washington
719 University School of Medicine in St. Louis), L. Zon (Harvard University), S. Kucenas
720 (University of Virginia), and D.A. Lyons (University of Edinburg).
721 This research was supported by a WHOI Von Damm and Ocean Ridge Initiative Fellowships to
722 J.M.P. and the Woods Hole Center for Oceans and Human Health (NIH: P01ES021923 and
723 P01ES028938; NSF: OCE-1314642 and OCE-1840381). This paper includes data submitted by

J.M.P. in partial fulfillment of the requirements for the degree of Doctor of Philosophy in Oceanography and Applied Ocean Science and Engineering at the Massachusetts Institute of Technology and the Woods Hole Oceanographic Institution (Panlilio, 2019)

COMPETING INTERESTS

The authors declare no competing interests.

REFERENCES

Almeida, R. G., Czopka, T., Ffrench-Constant, C. and Lyons, D. A. (2011). Individual axons regulate the myelinating potential of single oligodendrocytes in vivo. *Development* **138**, 4443–50.

Anderson, D. M., Glibert, P. M. and Burkholder, J. M. (2002). Harmful algal blooms and eutrophication: Nutrient sources, composition, and consequences. *Estuaries* **25**, 704–726.

Bates, D., Mächler, M., Bolker, B. and Walker, S. (2015). Fitting Linear Mixed-Effects Models using lme4. *J. Stat. Softw.* **67**, 1–48.

Bates, S. S., Hubbard, K. A., Lundholm, N., Montresor, M. and Leaw, C. P. (2018). Pseudo-nitzschia, Nitzschia, and domoic acid: New research since 2011. *Harmful Algae* **79**, 3–43.

Benaglia, T., Chauveau, D., Hunter, D. and Young, D. (2009). mixtools: An R Package for Analyzing Finite Mixture Models. *J. Stat. Softw.* **32**, 1–29.

Bernard, P. B., MacDonald, D. S., Gill, D. A., Ryan, C. L. and Tasker, R. A. (2007). Hippocampal mossy fiber sprouting and elevated trkB receptor expression following systemic administration of low dose domoic acid during neonatal development. *Hippocampus* **17**, 1121–1133.

Brodie, E. C., Gulland, F. M. D., Greig, D. J., Hunter, M., Jaakola, J., Leger, J. S., Leighfield, T., Dolah, V. and M, F. (2006). Domoic acid causes reproductive failure in california sea lions (Zalophus Californianus). *Mar. Mammal Sci.* **22**, 700–707.

Burgess, H. A. and Granato, M. (2007a). Sensorimotor gating in larval zebrafish. *J. Neurosci.* **27**, 4984–94.

Burgess, H. A. and Granato, M. (2007b). Modulation of locomotor activity in larval zebrafish during light adaptation. *J. Exp. Biol.* **210**, 2526–39.

Cendes, F., Andermann, F., Carpenter, S., Zatorre, R. J. and Cashman, N. R. (1995). Temporal lobe epilepsy caused by domoic acid intoxication: Evidence for glutamate receptor-mediated excitotoxicity in humans. *Ann. Neurol.* **37**, 123–126.

Cianciolo Cosentino, C., Roman, B. L., Drummond, I. A. and Hukriede, N. A. (2010). Intravenous microinjections of zebrafish larvae to study acute kidney injury. *J. Vis. Exp.*

Clark, S., Hubbard, K. A., Anderson, D. M., McGillicuddy, D. J., Ralston, D. K. and Townsend, D. W. (2019). Pseudo-nitzschia bloom dynamics in the Gulf of Maine: 2012–2016. *Harmful Algae* **88**, 101656.

Czopka, T., Ffrench-Constant, C. and Lyons, D. A. (2013). Individual oligodendrocytes have only a few hours in which to generate new myelin sheaths in vivo. *Dev. Cell* **25**, 599–609.

Dakshinamurti, K., Sharma, S., Sundaram, M. and Watanabe, T. (1993). Hippocampal changes in developing postnatal mice following intrauterine exposure to domoic acid. *J. Neurosci.* **13**, 4486–4495.

Doucette, T. A., Bernard, P. B., Husum, H., Perry, M. A., Ryan, C. L. and Tasker, R. A. (2004). Low doses of domoic acid during postnatal development produce permanent changes in rat behaviour and hippocampal morphology. *Neurotox. Res.* **6**, 555–563.

Eaton, R. C., Bombardieri, R. A. and Meyer, D. L. (1977). The Mauthner-initiated startle response in teleost fish. *J. Exp. Biol.* **66**, 65–81.

Faber, D. S., Fetcho, J. R. and Korn, H. (1989). Neuronal Networks Underlying the Escape Response in Goldfish. *Ann. N. Y. Acad. Sci.* **563**, 11–33.

Gill, D. A., Bastlund, J. F., Watson, W. P., Ryan, C. L., Reynolds, D. S. and Tasker, R. A. (2010). Neonatal exposure to low-dose domoic acid lowers seizure threshold in adult rats.

Neuroscience **169**, 1789–1799.

Grant, K. S., Crouthamel, B., Kenney, C., McKain, N., Petroff, R., Shum, S., Jing, J., Isoherranen, N. and Burbacher, T. M. (2019). Preclinical modeling of exposure to a global marine bio-contaminant: Effects of in utero Domoic acid exposure on neonatal behavior and infant memory. *Neurotoxicol. Teratol.* **73**, 1–8.

Hampson, D. R. and Manalo, J. L. (1998). The activation of glutamate receptors by kainic acid and domoic acid. *Nat. Toxins* **6**, 153–8.

Higashijima, S., Masino, M. A., Mandel, G. and Fetcho, J. R. (2003). Imaging neuronal activity during zebrafish behavior with a genetically encoded calcium indicator. *J. Neurophysiol.* **90**, 3986–97.

Hoppmann, V., Wu, J. J., Søviknes, A. M., Helvik, J. V. and Becker, T. S. (2008). Expression of the eight AMPA receptor subunit genes in the developing central nervous system and sensory organs of zebrafish. *Dev. Dyn.* **237**, 788–99.

Hoshijima, K., Jurynec, M. J. and Grunwald, D. J. (2016). Precise Editing of the Zebrafish Genome Made Simple and Efficient. *Dev. Cell* **36**, 654–67.

Inoue, D. and Wittbrodt, J. (2011). One for all--a highly efficient and versatile method for fluorescent immunostaining in fish embryos. *PLoS One* **6**, e19713.

Jain, R. A., Wolman, M. A., Marsden, K. C., Nelson, J. C., Shoenhard, H., Echeverry, F. A., Szi, C., Bell, H., Skinner, J., Cobbs, E. N., et al. (2018). A Forward Genetic Screen in Zebrafish Identifies the G-Protein-Coupled Receptor CaSR as a Modulator of Sensorimotor Decision Making. *Curr. Biol.* **28**, 1357-1369.e5.

Jian Wang, G. H., Schmued, L. C., Andrews, A. M., Scallet, A. C., Slikker, W. H. and Binienda, Z. H. (2000). Systemic Administration of Domoic Acid-Induced Spinal Cord Lesions in Neonatal Rats. *J. Spinal Cord Med.* **23**, 31–39.

Kimmel, C. B., Powell, S. L. and Metcalfe, W. K. (1982). Brain neurons which project to the spinal cord in young larvae of the zebrafish. *J. Comp. Neurol.* **205**, 112–127.

Kohashi, T. and Oda, Y. (2008). Initiation of Mauthner- or Non-Mauthner-Mediated Fast Escape Evoked by Different Modes of Sensory Input. *J. Neurosci.* **28**, 10641–10653.

Kohashi, T., Nakata, N. and Oda, Y. (2012). Effective Sensory Modality Activating an Escape Triggering Neuron Switches during Early Development in Zebrafish. *J. Neurosci.* **32**, 5810–5820.

Konietschke, F., Placzek, M., Schaarschmidt, F. and Hothorn, L. A. (2015). An R Software Package for Nonparametric Multiple Comparisons and Simultaneous Confidence Intervals. *J. Stat. Softw.* **64**, 1–17.

Korn, H. and Faber, D. S. (2005). The Mauthner cell half a century later: a neurobiological model for decision-making? *Neuron* **47**, 13–28.

Kucenas, S., Takada, N., Park, H.-C., Woodruff, E., Broadie, K. and Appel, B. (2008). CNS-derived glia ensheath peripheral nerves and mediate motor root development. *Nat. Neurosci.* **11**, 143–151.

Lefebvre, K. A., Hendrix, A., Halaska, B., Duignan, P., Shum, S., Isoherranen, N., Marcinek, D. J. and Gulland, F. M. D. (2018). Domoic acid in California sea lion fetal fluids indicates continuous exposure to a neuroteratogen poses risks to mammals. *Harmful Algae* **79**, 53–57.

Levin, E. D., Pizarro, K., Pang, W. G., Harrison, J. and Ramsdell, J. S. (2005). Persisting behavioral consequences of prenatal domoic acid exposure in rats. *Neurotoxicol. Teratol.* **27**, 719–25.

Lewinski, F. von and Keller, B. U. (2005). Ca2+, mitochondria and selective motoneuron vulnerability: implications for ALS. *Trends Neurosci.* **28**, 494–500.

Longair, M. H., Baker, D. A. and Armstrong, J. D. (2011). Simple Neurite Tracer: open source software for reconstruction, visualization and analysis of neuronal processes. *Bioinformatics* **27**, 2453–2454.

Marquart, G. D., Tabor, K. M., Bergeron, S. A., Briggman, K. L. and Burgess, H. A. (2019). Prepontine non-giant neurons drive flexible escape behavior in zebrafish. *PLOS Biol.* **17**, e3000480.

Marsden, K. C. and Granato, M. (2015). In Vivo Ca(2+) Imaging Reveals that Decreased Dendritic Excitability Drives Startle Habituation. *Cell Rep.* **13**, 1733–40.

Maucher, J. M. and Ramsdell, J. S. (2005). Domoic acid transfer to milk: evaluation of a potential route of neonatal exposure. *Environ. Health Perspect.* **113**, 461–4.

Maucher, J. M. and Ramsdell, J. S. (2007). Maternal-fetal transfer of domoic acid in rats at two gestational time points. *Environ. Health Perspect.* **115**, 1743–6.

McKeown, K. A., Moreno, R., Hall, V. L., Ribera, A. B. and Downes, G. B. (2012). Disruption of Eaat2b, a glutamate transporter, results in abnormal motor behaviors in developing zebrafish. *Dev. Biol.* **362**, 162–71.

McKibben, S. M., Peterson, W., Wood, A. M., Trainer, V. L., Hunter, M. and White, A. E. (2017). Climatic regulation of the neurotoxin domoic acid. *Proc. Natl. Acad. Sci. U. S. A.* **114**, 239–244.

McLean, D. L. and Dougherty, K. J. (2015). Peeling back the layers of locomotor control in the spinal cord. *Curr. Opin. Neurobiol.* **33**, 63–70.

Mills, B. D., Pearce, H. L., Khan, O., Jarrett, B. R., Fair, D. A. and Lahvis, G. P. (2016). Prenatal domoic acid exposure disrupts mouse pro-social behavior and functional connectivity MRI. *Behav. Brain Res.* **308**, 14–23.

Mirjany, M., Preuss, T. and Faber, D. S. (2011). Role of the lateral line mechanosensory system in directionality of goldfish auditory evoked escape response. *J. Exp. Biol.* **214**, 3358–3367.

Moens, C. B., Yan, Y. L., Appel, B., Force, A. G. and Kimmel, C. B. (1996). valentino: a zebrafish gene required for normal hindbrain segmentation. *Development* **122**, 3981–90.

Myers, P. Z. (1985). Spinal motoneurons of the larval zebrafish. *J. Comp. Neurol.* **236**, 555–561.

Nicolson, T. (2017). The genetics of hair-cell function in zebrafish. *J. Neurogenet.* **31**, 102–112.

Nicolson, T., Rüsch, A., Friedrich, R. W., Granato, M., Ruppersberg, J. P. and Nüsslein-Volhard, C. (1998). Genetic Analysis of Vertebrate Sensory Hair Cell Mechanosensation: the Zebrafish Circler Mutants. *Neuron* **20**, 271–283.

O'Malley, D. M., Kao, Y. H. and Fetcho, J. R. (1996). Imaging the functional organization of zebrafish hindbrain segments during escape behaviors. *Neuron* **17**, 1145–55.

Panlilio, J. M. (2019). Impacts of developmental exposures to the harmful algal bloom toxin domoic acid on neural development and behavior.

Panlilio, J. M., Aluru, N. and Hahn, M. E. (2020). Developmental Neurotoxicity of the Harmful Algal Bloom Toxin Domoic Acid: Cellular and Molecular Mechanisms Underlying Altered Behavior in the Zebrafish Model. *Environ. Health Perspect.* **128**, 117002.

Patten, S. A. and Ali, D. W. (2007). AMPA receptors associated with zebrafish Mauthner cells switch subunits during development. *J. Physiol.* **581**, 1043–56.

Perry, M. A., Ryan, C. L. and Tasker, R. A. (2009). Effects of low dose neonatal domoic acid administration on behavioural and physiological response to mild stress in adult rats. *Physiol. Behav.* **98**, 53–59.

Petroff, R., Richards, T., Crouthamel, B., McKain, N., Stanley, C., Grant, K. S., Shum, S., Jing, J., Isoherranen, N. and Burbacher, T. M. (2019). Chronic, Low-Level Oral Exposure to Marine Toxin, Domoic Acid, Alters Whole Brain Morphometry in Nonhuman Primates. *Neurotoxicology*.

Pogoda, H.-M., Sternheim, N., Lyons, D. A., Diamond, B., Hawkins, T. A., Woods, I. G., Bhatt, D. H., Franzini-Armstrong, C., Dominguez, C., Arana, N., et al. (2006). A genetic screen identifies genes essential for development of myelinated axons in zebrafish. *Dev. Biol.* **298**, 118–31.

Ripley, B., Venables, B., Bates, D. M., Hornik, J., Gebhardt, A. and Firth, D. (2018). *Package "MASS."*

Rust, L., Gulland, F., Frame, E. and Lefebvre, K. (2014). Domoic acid in milk of free living California marine mammals indicates lactational exposure occurs. *Mar. Mammal Sci.* **30**, 1272–1278.

Sebe, J. Y., Cho, S., Sheets, L., Rutherford, M. A., Henrique Von Gersdorff, X. and Raible, D. W. (2017). Ca 2-Permeable AMPARs Mediate Glutamatergic Transmission and Excitotoxic Damage at the Hair Cell Ribbon Synapse.

Sheets, L. (2017). Excessive activation of ionotropic glutamate receptors induces apoptotic hair-cell death independent of afferent and efferent innervation. *Sci. Rep.* **7**, 41102.

Shiotani, M., Cole, T. B., Hong, S., Park, J. J. Y., Griffith, W. C., Burbacher, T. M., Workman, T., Costa, L. G. and Faustman, E. M. (2017). Neurobehavioral assessment of mice following repeated oral exposures to domoic acid during prenatal development. *Neurotoxicol. Teratol.* **64**, 8–19.

Shum, S., Jing, J., Petroff, R., Crouthamel, B., Grant, K. S., Burbacher, T. M. and Isoherranen, N. (2020). Maternal-fetal disposition of domoic acid following repeated oral dosing during pregnancy in nonhuman primate. *Toxicol. Appl. Pharmacol.* **398**, 115027.

Soroldoni, D., Hogan, B. M. and Oates, A. C. (2009). Simple and Efficient Transgenesis with Meganuclease Constructs in Zebrafish.pp. 117–130. Humana Press.

Tabor, K. M., Bergeron, S. A., Horstick, E. J., Jordan, D. C., Aho, V., Porkka-Heiskanen, T., Haspel, G. and Burgess, H. A. (2014). Direct activation of the Mauthner cell by electric field pulses drives ultra-rapid escape responses 2 3 4. *J Neurophysiol*.

Tanemura, K., Igarashi, K., Matsugami, T.-R., Aisaki, K., Kitajima, S. and Kanno, J. (2009). Intrauterine environment-genome interaction and Children's development (2): Brain structure impairment and behavioral disturbance induced in male mice offspring by a single intraperitoneal administration of domoic acid (DA) to their dams. *J. Toxicol. Sci.* **34**, SP279–SP286.

Teitelbaum, J. S., Zatorre, R. J., Carpenter, S., Gendron, D., Evans, A. C., Gjedde, A. and Cashman, N. R. (1990). Neurologic sequelae of domoic acid intoxication due to the ingestion of contaminated mussels. *N. Engl. J. Med.* **322**, 1781–7.

Thermes, V., Grabher, C., Ristoratore, F., Bourrat, F., Choulika, A., Wittbrodt, J. and Joly, J.-S. (2002). I-SceI meganuclease mediates highly efficient transgenesis in fish. *Mech. Dev.* **118**, 91–8.

Tiedeken, J. A. and Ramsdell, J. S. (2007). Embryonic exposure to domoic acid increases the susceptibility of zebrafish larvae to the chemical convulsant pentylenetetrazole. *Environ.*

Health Perspect. **115**, 1547–52.
Todd, K. J., Slatter, C. A. B. and Ali, D. W. (2004). Activation of Ionotropic Glutamate Receptors on Peripheral Axons of Primary Motoneurons Mediates Transmitter Release at the Zebrafish NMJ. *J. Neurophysiol.* **91**, 828–840.
Troconis, E. L., Ordoobadi, A. J., Sommers, T. F., Aziz-Bose, R., Carter, A. R. and Trapani, J. G. (2016). Intensity-dependent timing and precision of startle response latency in larval zebrafish. *J. Physiol.*
Tryphonas, L., Truelove, J., Nera, E. and Iverson, F. (1990). Acute Neurotoxicity of Domoic Acid in the Rat. *Toxicol. Pathol.* **18**, 1–9.
Turner, K. J., Bracewell, T. G. and Hawkins, T. A. (2014). Anatomical Dissection of Zebrafish Brain Development.pp. 197–214. Humana Press, Totowa, NJ.
Wang, G. J., Schmued, L. C., Andrews, A. M., Scallet, A. C., Slikker, W. and Binienda, Z. (2000). Systemic administration of domoic acid-induced spinal cord lesions in neonatal rats. *J. Spinal Cord Med.* **23**, 31–9.
Warp, E., Agarwal, G., Wyart, C., Friedmann, D., Oldfield, C. S., Conner, A., Del Bene, F., Arrenberg, A. B., Baier, H. and Isacoff, E. Y. (2012). Emergence of patterned activity in the developing zebrafish spinal cord. *Curr. Biol.* **22**, 93–102.
Wekell, J. C., Jurst, J. and Lefebvre, K. A. (2010). The origin of the regulatory limits for PSP and ASP toxins in shellfish. *J. Shellfish Res.* **23**, 927–930.
Wobbrock, J. O., Findlater, L., Gergle, D. and Higgins, J. J. (2011). The aligned rank transform for nonparametric factorial analyses using only anova procedures. In *Proceedings of the 2011 annual conference on Human factors in computing systems - CHI 2011*, p. 143. New York, New York, USA: ACM Press.
Wolman, M. A., Jain, R. A., Liss, L. and Granato, M. (2011). Chemical modulation of memory formation in larval zebrafish. *Proc. Natl. Acad. Sci. U. S. A.* **108**, 15468–73.
Xi, D., Peng, Y. G. and Ramsdell, J. S. (1997). Domoic acid is a potent neurotoxin to neonatal rats. *Nat. Toxins* **5**, 74–9.
Zottoli, S. J. (1977). Correlation of the startle reflex and Mauthner cell auditory responses in unrestrained goldfish. *J. Exp. Biol.* **66**, 243–254.
Zuloaga, D. G., Lahvis, G. P., Mills, B., Pearce, H. L., Turner, J. and Raber, J. (2016). Fetal domoic acid exposure affects lateral amygdala neurons, diminishes social investigation and alters sensory-motor gating. *Neurotoxicology* **53**, 132–140.

FIGURE CAPTIONS

Figure 1: Domoic acid-exposed larvae are less responsive and preferentially perform LLC startles compared to controls when given auditory/vibrational stimuli.

(A) Distribution of fish that did one of three behaviors: 1) no response, 2) LLC startle, or 3) SLC startle for each stimulus intensity. Only the first of the 4 replicate stimuli were graphed so that each fish is represented once. Individual points represent single fish that performed each behavior. Large black dots represent the proportion of the population that performed one of the three behaviors within a given stimulus intensity. Asterisks in the no response column represent statistically significant differences in responsiveness in DomA-exposed fish relative to controls within each stimulus intensity. Asterisks in the SLC column represent statistically significant differences in the performance of SLC rather than LLCs in DomA-exposed fish relative to controls within each stimulus intensity. Significance was determined using mixed effects logistic regression. *$p < 0.05$, *** $p< 0.001$

(B) Relative Startle Bias Index was calculated for all fish that were responsive. Individual fish were provided with 4 replicate stimuli within a given stimulus intensity. Bias per individual was calculated as the (frequency of SLC – frequency of LLC)/ total responses. +1 represents the value in which all responses were SLC-type startles, and -1 represents the value in which all were LLC-type startles. Mean behavioral biases for a treatment group per stimulus intensity were graphed. Asterisks indicate statistical significance in performing SLC startles (versus LLC startles).

(C) Domoic acid-treated larvae were also classified by myelin category (0-3) in a subset of the experiments (subset of fish graphed in Figure 1B). Startle bias per myelin phenotype was plotted.

Figure 2: Kinematics deficits in auditory/vibrational startle are correlated to myelin defects.

(A) DomA-treated fish were further subcategorized by myelin sheath defects. 0 = control-like myelin sheaths to 3 = the most severe myelin defect observed. Bend angles during SLC startles with increasing stimulus intensities.

(B) Maximal angular velocities (Mav) during SLC startles with increasing stimulus intensities.

(C) Bend angles during LLC startles with increasing stimulus intensities.

(D) Maximal angular velocities (Mav) during LLC startles with increasing stimulus intensities.

Asterisks represent statistical significance between DomA and controls determined using an Aligned Ranked Transformed ANOVA test (* = $p <0.05$, ** = $p< 0.001$, *** = $p < 0.0001$).

Figure 3: Domoic acid-exposed larvae have aberrant startle responses to direct electrical stimulation.

(A) Larvae were head-mounted in agar and positioned rostral-caudally to the electrodes. Control larvae were mounted on the left, DomA-exposed larvae on the right. Larvae were then provided with a 6 Volt, 2 millisecond (ms) square pulse. Their tail movements were captured using a high-speed video camera.

(B) Percent responsiveness of individual larvae to 7 identical electric field pulses. Points represent the percent of times an individual fish responded to replicate stimuli. 70/74 of the

control population responded 100% of the time while 47/74 of DomA-treated population responded 0% of the time.

(C) Latency distributions for control and DomA-treated fish. Count represents the number of fish that have latencies within each of the 2 ms time bins. The majority of the control fish responded within 2 ms after stimulus was produced (51/74 Control fish had a median latency of 1-2 ms). Not shown= 1 DomA-treated larva that responded at 179 ms.

(D) Maximal bend angle for control (n= 74) versus DomA-treated fish (n= 27). Each point represents the median response of an individual fish.

(E) Maximal angular velocity for control versus DomA-treated fish. Each point represents the median response of an individual fish.

***$p \leq 0.0001$ indicates significant difference between DomA-exposed fish relative to control fish. Statistical significance was determined using a nonparametric Behrens-Fisher t-test.

Figure 4: Severity in myelin defects is correlated with startle kinematic deficits from direct electric field stimulation.

(A) Representative widefield epifluoresence images of the myelin sheath phenotypes categorized, with (0) having no myelin defect to (3) having the most myelin severe defect observed. C0 = Control, D0- D3= DomA treated.

(B) Latency distributions for control and DomA-treated fish. The same data used in Figure 5C but further categorized by myelin sheath imaging categories. Not shown= 1 DomA-treated larvae which responded at 179 ms.

(C) Maximum bend angle for control (n=74) versus DomA-treated fish (n=25). Fish with myelin defects in category 1 were excluded from this analysis due to low sample sizes (n=2).

(D) Maximal angular velocity for control versus DomA-treated fish.

(E) Percent responsiveness of individual larvae to 7 identical electric field pulses. Points represent the percent of times an individual fish responded to replicate stimuli. Ratios listed above a group of points represent the ratio of fish that responded to that stimulus over the total within that percentage bracket. Ratios were listed when all the individual points could not fit on the graph.

Asterisks represent statistical significance between DomA and controls determined using the a nonparametric multiple comparisons test with Dunnett-type intervals

*** = $p < 0.0001$).

Figure 5: The sensory inputs required for the startle response appeared intact in domoic acid-exposed fish.

(A-B) DASPEI labeling of sensory neuromasts in 5 dpf larvae.

(A) Representative widefield fluorescence images of DASPEI-stained control and DomA-exposed larvae.

(B) Diagram of a 5-dpf larva with head neuromasts colored in teal and trunk neuromasts colored in peach. Head and trunk neuromast counts for control and DomA-exposed. Single points represent individual larvae. Black bar represents standard error of the mean (SE).

For cranial region, control – mean = 19 ± 2 (SD), DomA – mean = 19 ± 3 (SD)

For trunk region, control – mean =17, ± 2 (SD), DomA – mean = 17 ± 3 (SD) **(C-E)** Imaging of sensory ganglia in 5 dpf *Tg(cntn1b:EGFP-CAAX)* larvae.

(C) Diagram of a laterally mounted *Tg(cntn1b:EGFP-CAAX)* larva, with green boxes that indicate approximate areas imaged.

(D) Representative confocal images from the cranial region of laterally mounted *Tg(cntn1b:EGFP-CAAX)* control (n=33) and DomA-exposed (n=45) larvae. Inner ear is outlined in teal.

(E) Representative confocal images from anterior spinal cord in laterally mounted *Tg(cntn1b:EGFP-CAAX)* control (left; n=36) and DomA-exposed (right; n=46) larvae. Pink arrowhead points to a neuromast. pLL = peripheral lateral line.

Scale bars: 100 µm.

Figure 6: The majority of reticulospinal neurons required for startle responses are absent in domoic acid-exposed larvae.

(A) 7 dpf larvae were backfilled with Texas Red dextran through spinal cord transections. The figures represent the range of phenotypes observed in control and DomA-injected fish. Teal arrows mark Mauthner cells and magenta arrows mark backfilled neurons in rhombomere 5 (r5) and rhombomere (r6).

(B) Mauthner cells on the two lateral sides were scored per fish. A majority of DomA-exposed fish (identified 51 out of 60) did not have any Mauthner cells.

(C) Other reticulospinal neurons involved in startle responses (MiD2cm, MiD3) are located in r5 and r6. The presence of any neuron backfilled in r5 and r6 on the two lateral sides was scored. A majority of DomA-exposed fish had one or no neurons that were backfilled in this r5 and r6 (44 out of 60).

Statistical significance was determined using ordered logistic regression. Scale bar = 50 µm.

Figure 7: The majority of DomA-exposed larvae do not have Mauthner cells but have other hindbrain and midbrain structures

(A) Schematic of brains stained with 3A10, with labels for the Mauthner cells, medial longitudinal fasciculus, and hindbrain axonal tracts.

(B) Representative images of control and DomA-exposed brain tissue stained with 3A10. Teal arrow points to Mauthner cell. Scale bar = 100 microns

(C) Score of the number of Mauthner cells (0-2) present in control and treated larvae. Numbers within each section represent the number of larvae with the given phenotype.

(D) Score of the number of hindbrain axonal tracts detectable in control and treated larvae. Numbers within each section represent the number of larvae with the given phenotype.

Figure 8: Domoic acid exposure reduces axon collateral branching in primary motor neurons.

(A-B) Immunostaining for acetylated tubulin in 2.5 dpf embryos

(A) Diagram of a 2.5 dpf larvae laterally mounted and immunostained with α-acetylated tubulin. Anatomical features of interest are highlighted (PLL= peripheral lateral line, CaP= caudal primary motor neurons).

(B) Immunostaining with α-acetylated tubulin at 2.5 dpf. DomA-exposed embryos (n=34) had visible CaP axons, sensory neuron cell bodies, and PLLs that were indistinguishable from controls (n=31).

(C) Higher resolution image of control and DomA-exposed fish immunostained with α-acetylated tubulin

(C-D) Imaging of primary motor neuron branching in 2.5 dpf *Tg(cntn1b:EGFP-CAAX)* embryos

(D) Representative images from 5 dpf *Tg(cntn1b:EGFP-CAAX)* controls and DomA-exposed larvae taken at high resolution.

(E) Representative images from 5 dpf *Tg(cntn1b:EGFP-CAAX)* controls and DomA-exposed larvae used for tracing studies. Green arrow points to motor neuron axons that were traced to estimate primary motor neuron axonal lengths in each treatment. Tracings are false colored. The main primary motor neuron axon was traced in green, and the axon collaterals were traced with magenta.

(F) Quantification of total lengths from axonal tracings of a subset of the imaged fish (inclusive of the main motor neuron in green and axon collaterals in magenta). Each point represents a single axon in one fish (control n= 43, DomA n=45). Error bars represent standard error of the mean.

Statistical significance was determined using a one-way analysis of variance (ANOVA) *** = $p < 2.2e-16$. Scale bars = 100 µm.

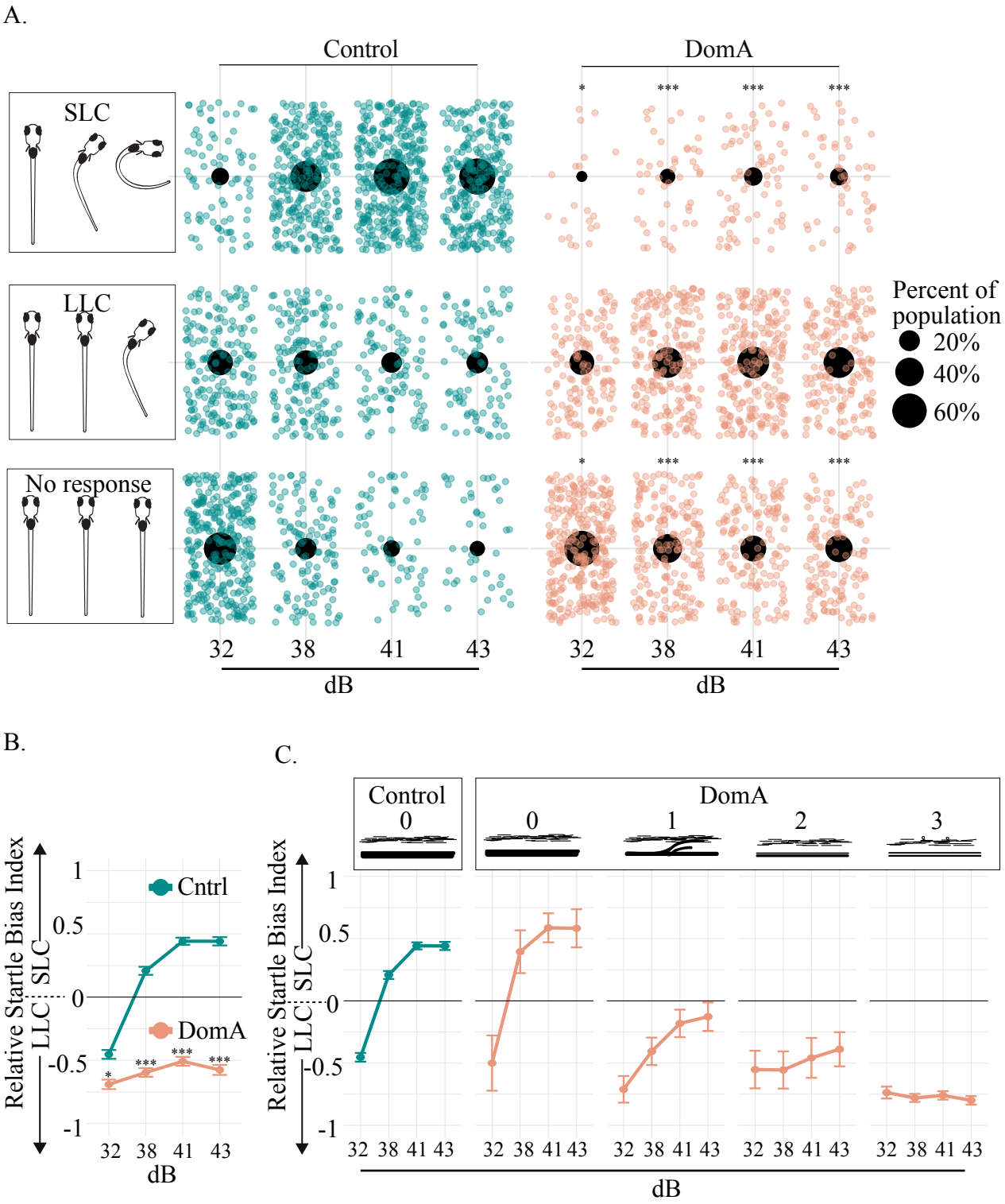

Figure 1: Domoic acid-exposed larvae are less responsive and preferentially perform LLC startles compared to controls when given auditory/vibrational stimuli.

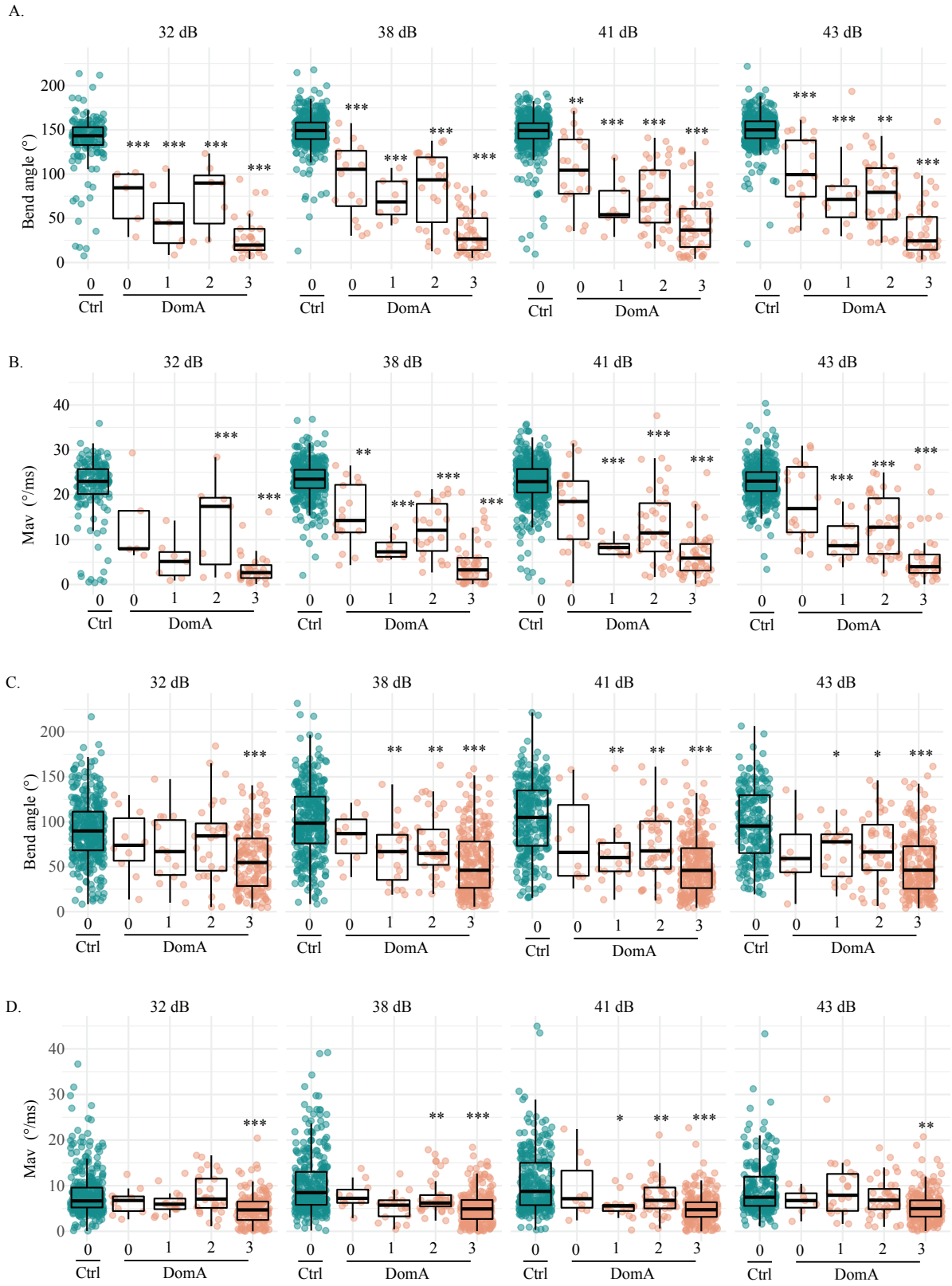

Figure 2: Kinematics deficits in auditory/vibrational startle are correlated to myelin defects.

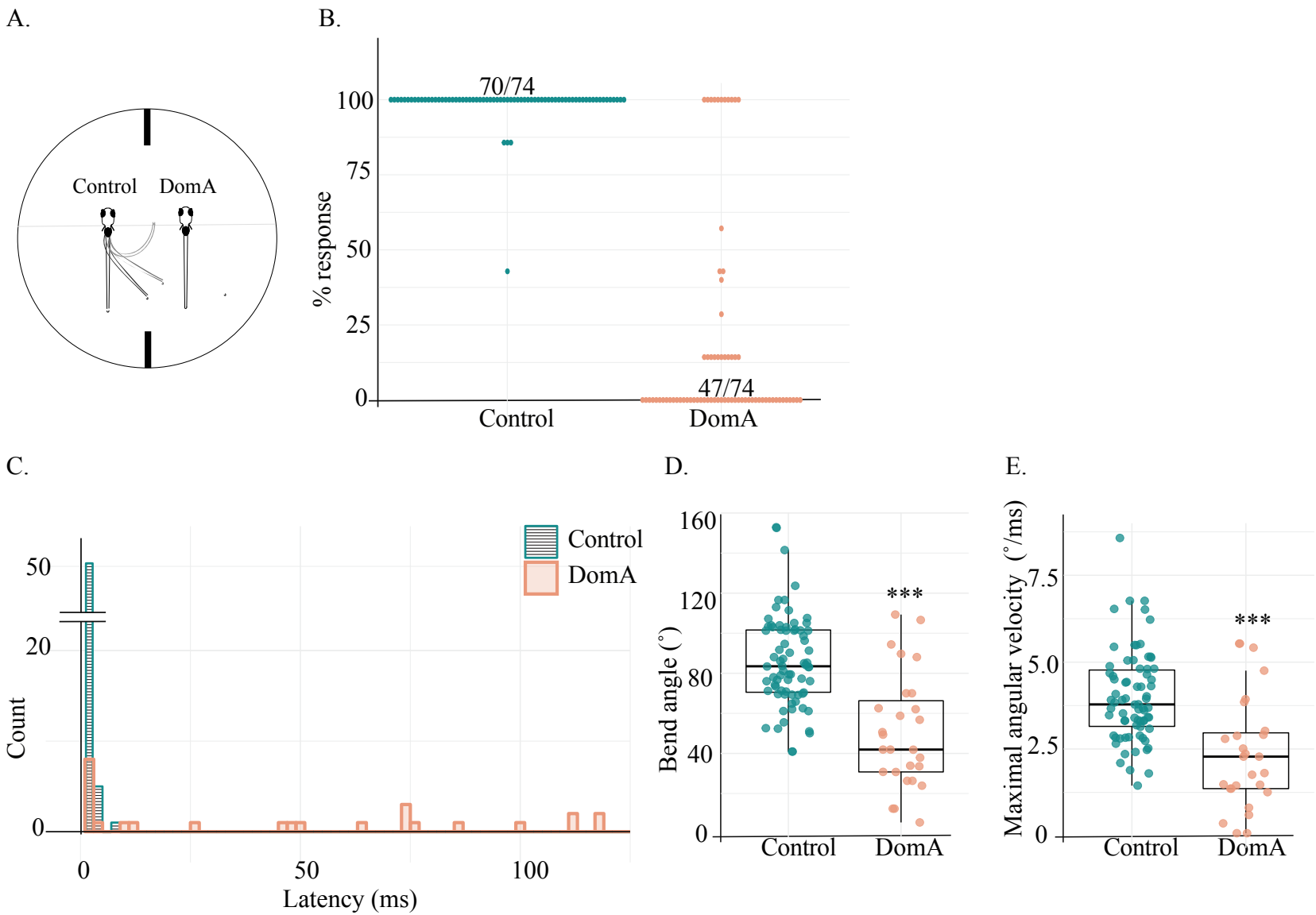

Figure 3: Domoic acid-exposed larvae have aberrant startle responses to direct electrical stimulation.

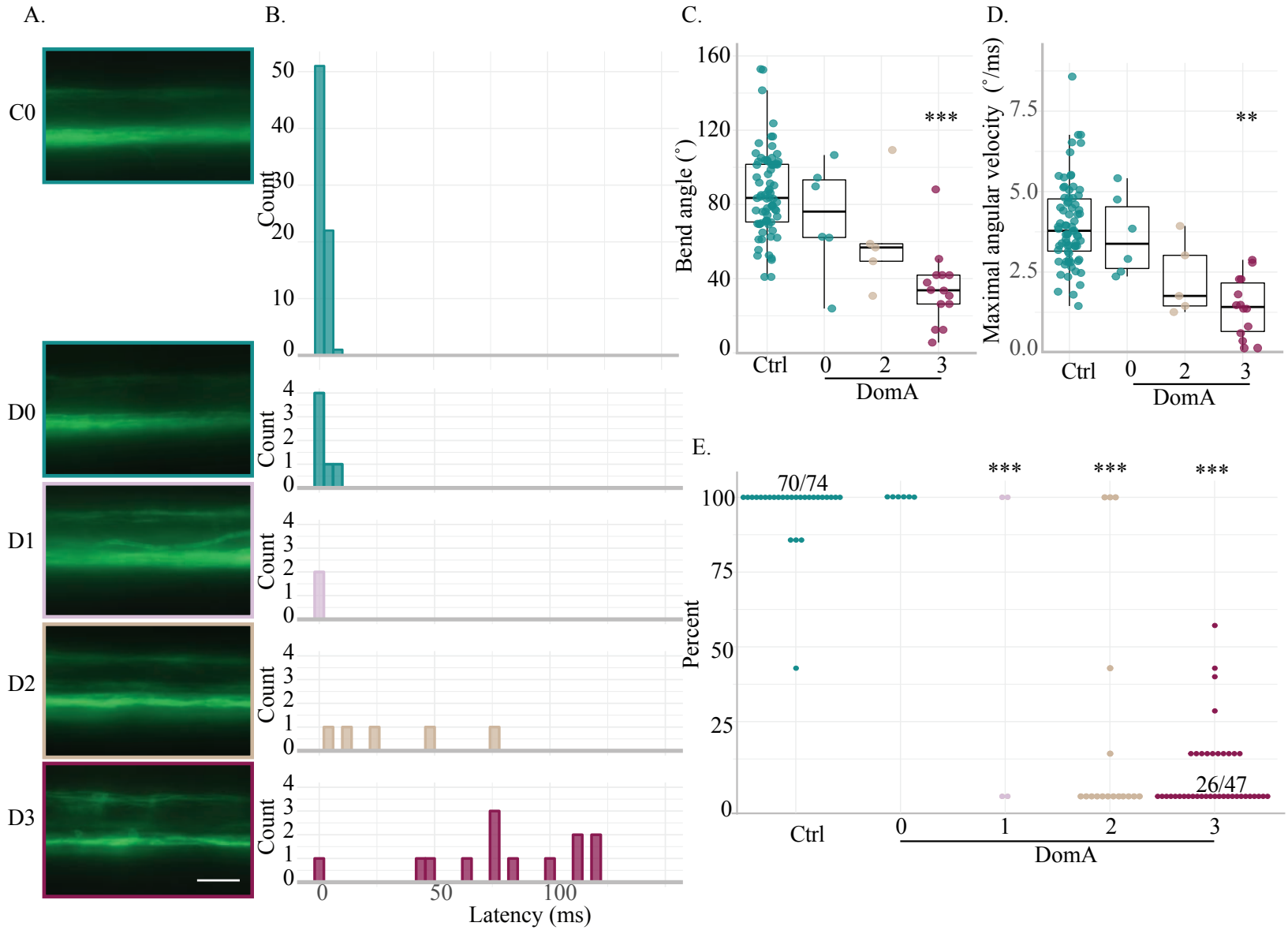

Figure 4: Severity in myelin defects is correlated with startle kinematic deficits from direct electric field stimulation.

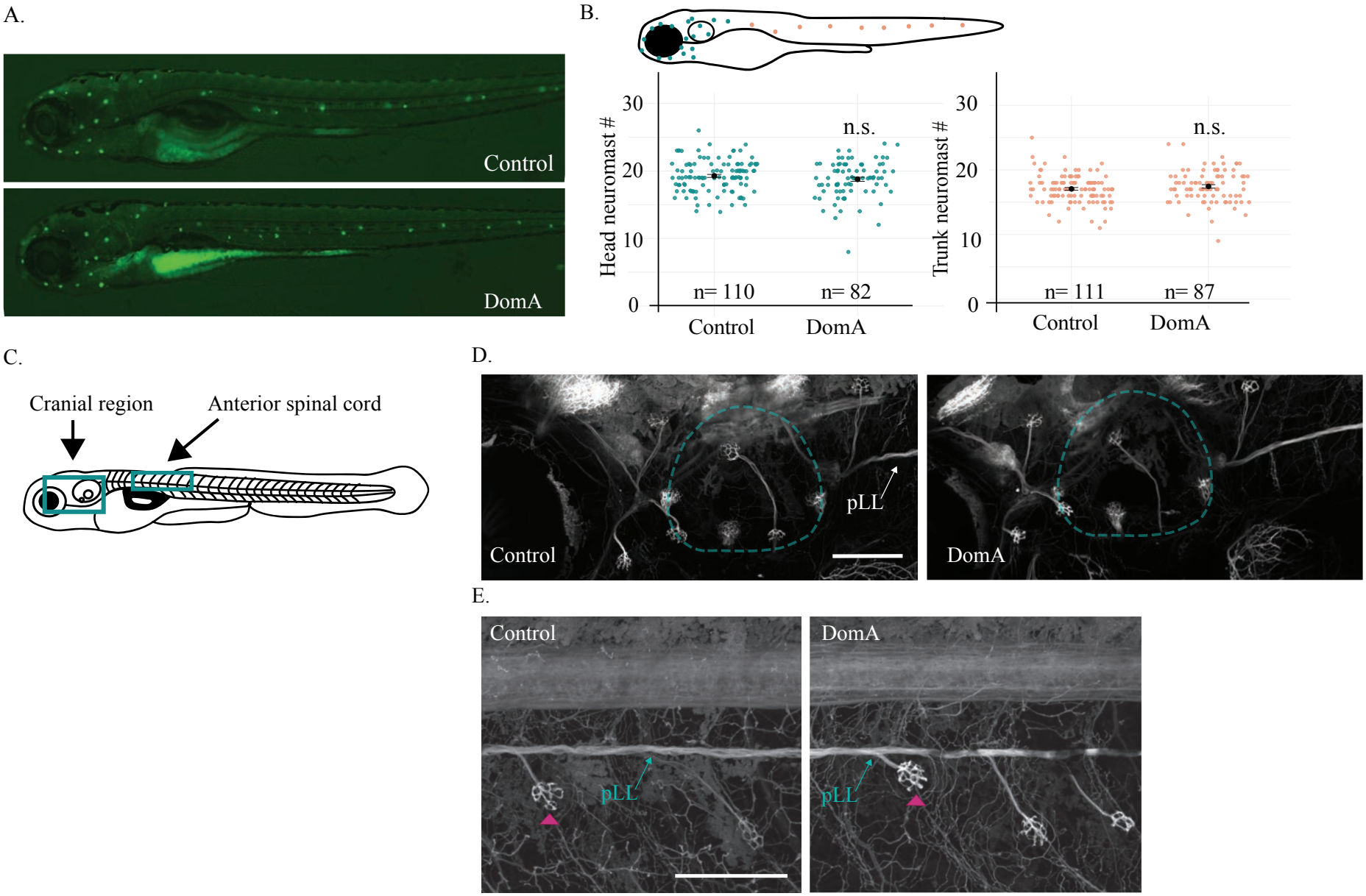

Figure 5: The sensory inputs required for the startle response appeared intact in domoic acid-exposed fish.

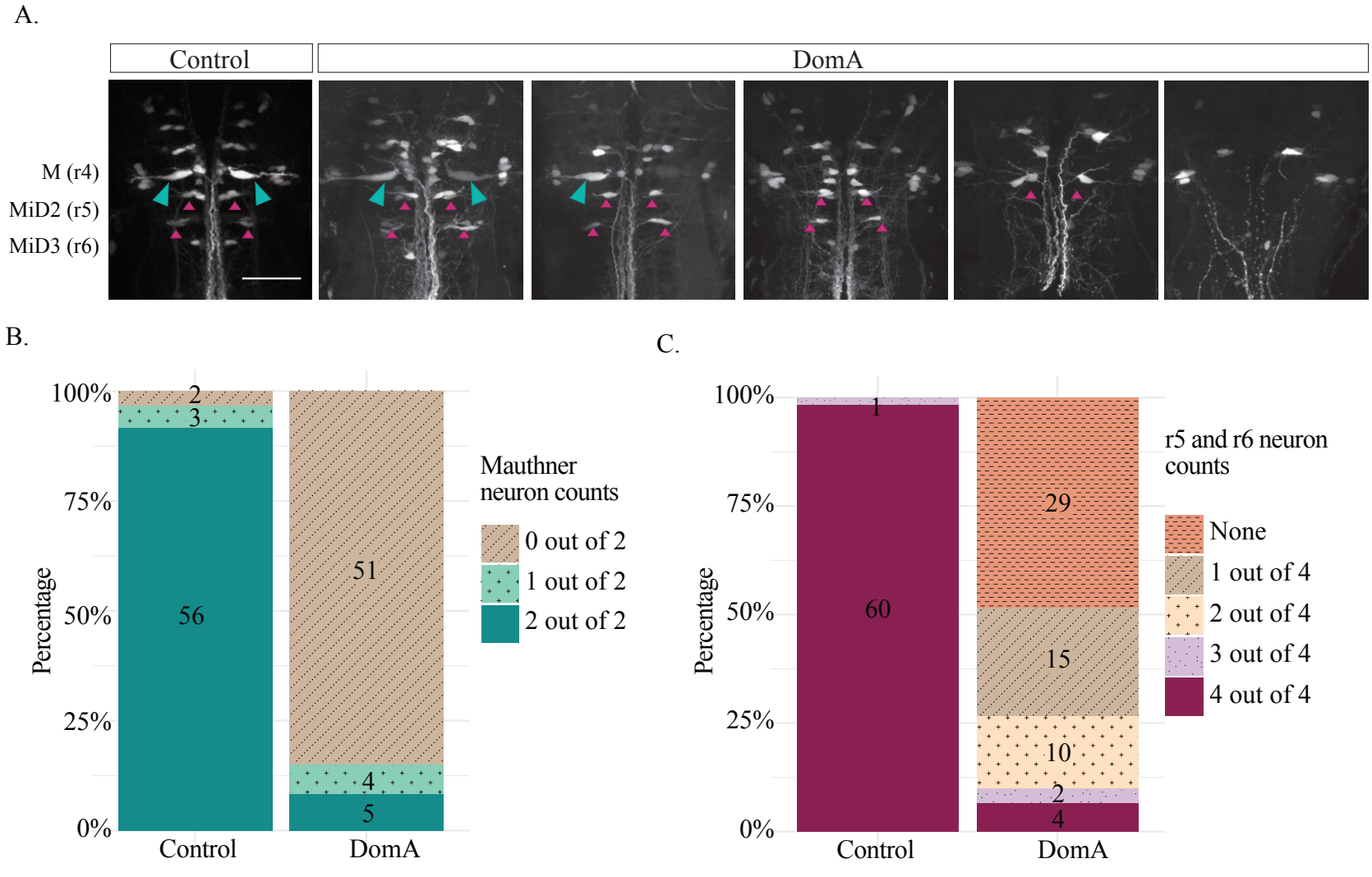

Figure 6: The majority of reticulospinal neurons required for startle responses are absent in domoic acid-exposed larvae.

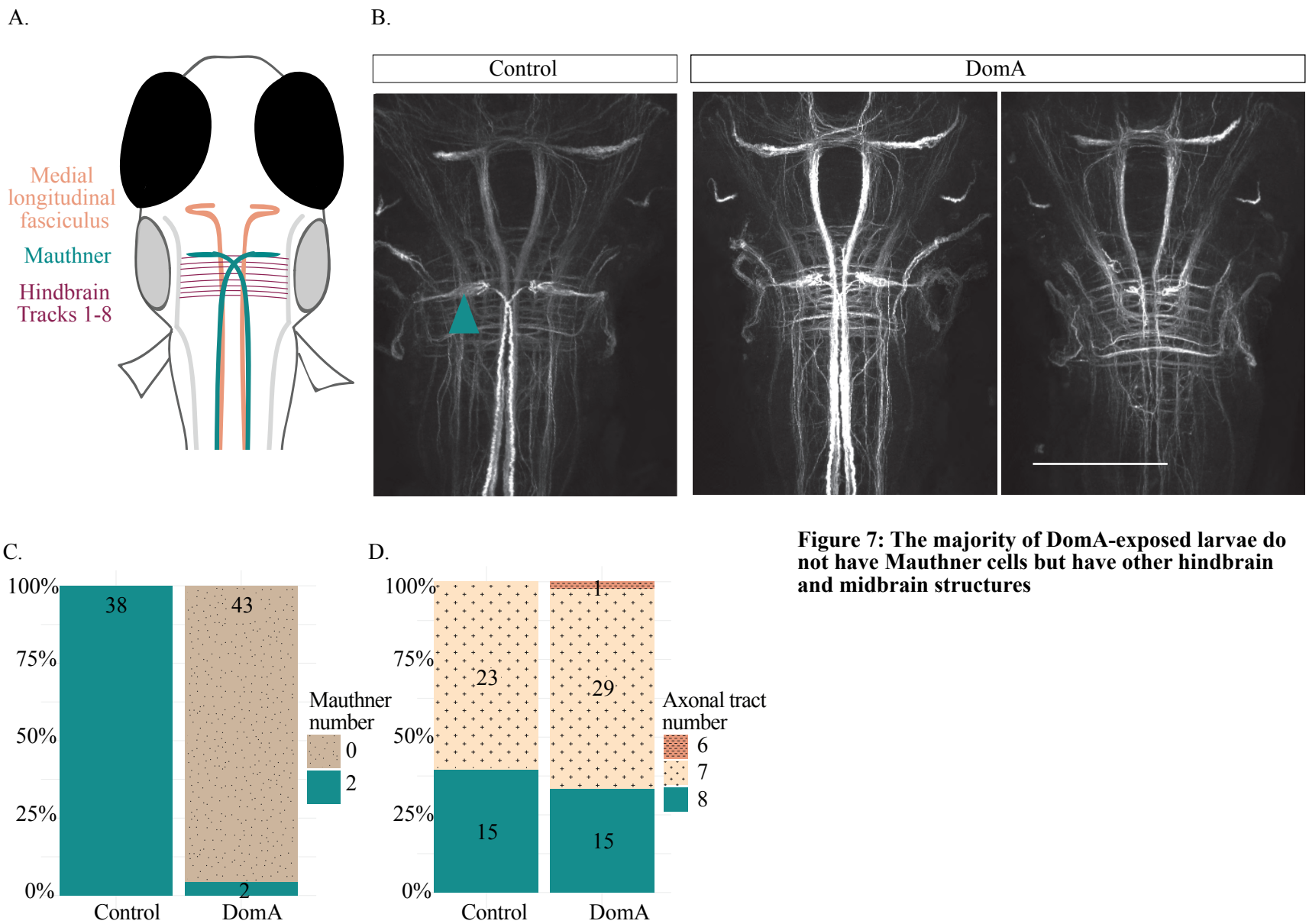

Figure 7: The majority of DomA-exposed larvae do not have Mauthner cells but have other hindbrain and midbrain structures

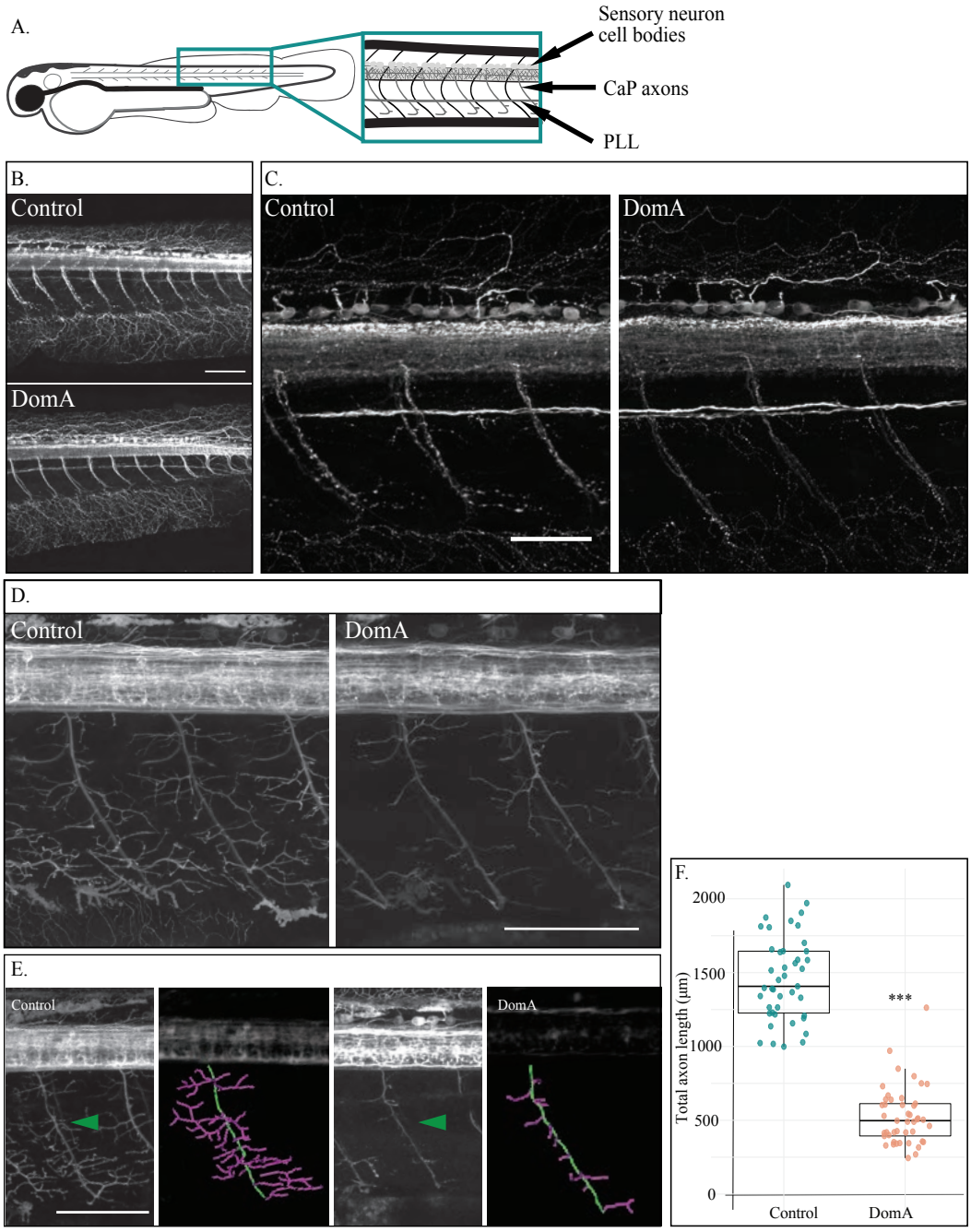

Figure 8: Domoic acid exposure reduces axon collateral branching in primary motor neurons.